


# Convergence patterns and rates in two-state perturbation expansions

Cite as: J. Chem. Phys. **151**, 084108 (2019); <https://doi.org/10.1063/1.5110554>

Submitted: 18 May 2019 . Accepted: 29 July 2019 . Published Online: 28 August 2019

Jeppe Olsen , and Poul Jørgensen



View Online



Export Citation



CrossMark

## ARTICLES YOU MAY BE INTERESTED IN

[Cluster perturbation theory. I. Theoretical foundation for a coupled cluster target state and ground-state energies](#)

The Journal of Chemical Physics **150**, 134108 (2019); <https://doi.org/10.1063/1.5004037>

[Adventures in DFT by a wavefunction theorist](#)

The Journal of Chemical Physics **151**, 160901 (2019); <https://doi.org/10.1063/1.5116338>

[In search of Coulson's lost theorem](#)

The Journal of Chemical Physics **151**, 151101 (2019); <https://doi.org/10.1063/1.5128624>

Lock-in Amplifiers  
up to 600 MHz



# Convergence patterns and rates in two-state perturbation expansions

Cite as: J. Chem. Phys. 151, 084108 (2019); doi: 10.1063/1.5110554

Submitted: 18 May 2019 • Accepted: 29 July 2019 •

Published Online: 28 August 2019



View Online



Export Citation



CrossMark

Jeppe Olsen<sup>a)</sup>  and Poul Jørgensen<sup>b)</sup>

## AFFILIATIONS

Department of Chemistry, Aarhus University, Langelandsgade 140, DK-8000 Aarhus C, Denmark

<sup>a)</sup> Electronic mail: [jeppe@chem.au.dk](mailto:jeppe@chem.au.dk)

<sup>b)</sup> Electronic mail: [pou@chem.au.dk](mailto:pou@chem.au.dk)

## ABSTRACT

A simple two-state model has previously been shown to be able to describe and rationalize the convergence of the most common perturbation method for including electron correlation, the Møller-Plesset expansion. In particular, this simple model has been able to predict the convergence rate and the form of the higher-order corrections for typical Møller-Plesset expansions of the correlation energy. In this paper, the convergence of nondegenerate perturbation expansions in the two-state model is analyzed in detail for a general form of two-state perturbation expansion by examining the analytic expressions of the corrections and series of the values of the corrections for various choices of the perturbation. The previous analysis that covered only a single form of the perturbation is thereby generalized to arbitrary forms of the perturbation. It is shown that the convergence may be described in terms of four characteristics: archetype, rate of convergence, length of recurring period, and sign pattern. The archetype defines the overall form of a plot of the energy-corrections, and the remaining characteristics specify details of the archetype. For symmetric (Hermitian) perturbations, five archetypes are observed: zigzag, interspersed zigzag, triadic, ripples, and geometric. Two additional archetypes are obtained for an asymmetric perturbation: zigzag-geometric and convex-geometric. For symmetric perturbations, each archetype has a distinctive pattern that recurs with a period which depends on the perturbation parameters, whereas no such recurrence exists for asymmetric perturbations from a series of numerical corrections. The obtained relations between the form of a two-state perturbation and the energy corrections allow us to obtain additional insights into the convergence behavior of the Møller-Plesset and other forms of perturbation expansions. This is demonstrated by analyzing several diverging or slowly converging perturbation expansions of ground state and excitation energies. It is demonstrated that the higher-order corrections of these expansions can be described using the two-state model and each expansion can therefore be described in terms of an archetype and the other three characteristics. Examples of all archetypes except the zigzag and convex-geometric archetypes are given. For each example, it is shown how the characteristics may be extracted from the higher-order corrections and used to identify the term in the perturbation that is the cause of the observed slow convergence or divergence.

© 2019 Author(s). All article content, except where otherwise noted, is licensed under a Creative Commons Attribution (CC BY) license (<http://creativecommons.org/licenses/by/4.0/>). <https://doi.org/10.1063/1.5110554>

## I. INTRODUCTION

Quantum mechanical perturbation theory has since its introduction<sup>1</sup> been used to calculate a large number of interactions, including interactions between molecules and external fields, interactions between nonoverlapping molecules, as well as correlation contributions to energies and properties of molecules. In quantum chemistry, the perturbation method that has most extensively been used to describe electron correlation is Møller-Plesset

Perturbation Theory (MPPT),<sup>2-5</sup> which uses the Hartree-Fock state as the zeroth-order state and the Møller-Plesset partitioning of the Hamiltonian.

An important characteristic of a perturbation expansion is its asymptotic convergence: is the expansion convergent or divergent and what is the asymptotic convergence rate? An extensive mathematical literature exists on the subject of convergence of perturbation theory including the seminal work for general (infinite) linear operators<sup>6</sup> and for finite dimensional operators,<sup>7</sup> but it was through

numerical studies that insight into the convergence of MPPT was obtained. It was originally assumed that the MPPT perturbation expansion of an electronic wave function is convergent if the wave function is strongly dominated by its Hartree-Fock component. This assumption was corroborated by the first calculations of high-order energy corrections of MPPT.<sup>8</sup> However, the question of convergence turned out to be more complicated, and states that are strongly dominated by the Hartree-Fock state may diverge. The first indication that factors other than the dominance of the Hartree-Fock state is important for the convergence of the MPPT expansion was the observation that the expansion for molecules containing electron-rich atoms, such as fluorine, show a slow convergence with oscillating signs of the corrections.<sup>9</sup> Subsequent calculations of high-order terms of the MPPT series for HF and Ne showed that these series change from convergent to divergent expansions when diffuse basis functions are added to the basis sets<sup>10,11</sup> although the wave functions remain strongly dominated by the Hartree-Fock state. These divergences were surprising but have been observed in additional studies, including a test using 128 bit precision to examine the numerical stability of the series and divergences.<sup>12</sup>

The MPPT expansion has been generalized to a coupled cluster perturbation theory (CCPT), where the zeroth-order (parent) state is a coupled cluster state, the target state is another coupled cluster state with a larger excitation space, and the Hamiltonian partitioning is the standard Møller-Plesset partitioning.<sup>13,14</sup> The standard MPPT series is recovered by using a vanishing and full excitation space for the parent and target states, respectively. The CCPT methods give typically energies that are more accurate than those obtained using MPPT, but the accuracy at low order and the high-order convergence is impaired by the large errors associated with the use of the Fock-operator as the zeroth-order operator, in particular, when the complete or nearly complete coupled cluster target state is employed.<sup>15</sup> If a target state that includes quadruple or higher excitations is employed for an electron-rich molecule, the high-order terms have thus the same divergent behavior as MPPT.<sup>15</sup> However, improved high-order convergence and lower-order results may usually be obtained in these schemes by restricting the excitation level of the target state, thereby eliminating the multiple excited states that gives rise to the divergence of MPPT for molecules with electron-rich atoms.

Very recently, we have introduced the cluster perturbation (CP) methods.<sup>16–20</sup> These methods differ from the CCPT methods by their use of a zeroth-order Jacobian that includes the exact Jacobian in the parent excitation space and approximates the zeroth-order Jacobian for excitations outside the parent space with orbital energy differences. This leads to improved convergence of the perturbation expansion for ground state energies.<sup>16</sup> Another attractive feature of the CP expansions is that they can be extended to describe excitation energies and response properties.<sup>16,17</sup> The theoretical foundation for the analysis of the convergence of the CP series for reference energies, excitation energies, and molecular properties is developed in Ref. 18.

A formal difference between CP and CCPT on one hand and standard perturbation methods including MPPT on the other hand is that the perturbation matrix of the former are asymmetric, whereas the perturbation matrix is symmetric for standard perturbation methods. This motivates that we in the following also consider expansions with an asymmetric perturbation.

As mentioned above, the MPPT expansion of the energy exhibits a characteristic pattern for molecules containing electron-rich atoms. Other patterns for the high-order corrections have been observed and reported. The MPPT expansion for the ground state energy of  $C_2$  at the equilibrium geometry<sup>10,12</sup> exhibits a convergence pattern that in Ref. 12 was described as “a fascinating pattern of protracted, decaying ringing.” This pattern is often observed for the CCPT energy and CP energy and excitation energy series. Additional patterns have been observed for the ground and excited state energies using the CP series. The origin of these convergence patterns is presently unknown. It is the origin of these patterns and, in particular, their relations to the form of the perturbation that are the focal points of the present work. Although we will use MPPT, CPPT, and CP perturbation series as examples of perturbation expansions, our results are general.

The study of the convergence behavior of MPPT and other perturbation expansions in a finite-dimensional space is greatly simplified by noting that the correction vectors for these expansions becomes nearly linear dependent as the order of the corrections increase.<sup>8,21</sup> The higher-order convergence of these expansions may therefore be studied using a simple two-state expansion, including the ground state and the asymptotic correction vector. Such a two-state model was originally introduced by Chaudhuri, Finley, and Freed<sup>22</sup> and was further developed and applied to analyze the high-order convergence of the MPPT series.<sup>21</sup> In the latter analysis, the two-state model was considered for a symmetric perturbation as defined by two parameters: the gap-shift that gives the reduction in the energies of the zeroth-order states and the coupling of the two zeroth-order states. To accommodate the possibility of a general asymmetric two-state perturbation matrix, this simple form of the perturbation must be generalized. We will thus consider both a symmetric perturbation, where the two off-diagonal elements of the perturbation have the same sign and an asymmetric perturbation where the two off-diagonal elements have opposite signs. With these extended definitions of symmetric and asymmetric perturbations, it is possible to analyze perturbation expansions of coupled cluster states.

The two-state model with a symmetric perturbation has been analyzed in detail for the case, where the gap-shift is much larger than the coupling term. In particular, it has been shown that the observed divergences of MPPT for electron-rich atoms and molecules are caused by the large negative gap-shifts originating from the double counting of the electron-electron repulsion in the Fock-operator.<sup>21</sup>

To obtain an improved understanding of the convergence of perturbation series for electron correlation and to design improved perturbation methods, the relation between the observed patterns of the corrections and the dominating interactions in the Hamiltonian must be uncovered. For example, is the ringing pattern of the MPPT expansion for  $C_2$  due to large interactions between two or more states or is it caused by the large errors of the zeroth-order energies that are inherent in MPPT? To obtain this understanding, we will consider perturbation expansions using the two-state model for general choices of the coupling and gap-shift and analyze this model for symmetric as well as asymmetric perturbations. For symmetric perturbation, the relative size of the two parameters of the perturbation leads to five archetypes, which we denote zigzag, interspersed zigzag, triadic, ripple,

and zigzag convergence. In the zigzag and geometric archetypes, there are simple relations between two consecutive corrections, whereas the three other types have more complicated relations between the terms and exhibit recurring patterns over three or more orders. The convergence pattern for an asymmetric perturbation may belong to one of the two additional archetypes, the convex-geometric and zigzag-geometric archetypes or to either the zigzag or geometric archetypes.

The developed relations between the form of the archetypes and the underlying perturbation parameters can be used to extract estimates of the two perturbation parameters from the four characteristics of a calculated perturbation expansion: archetype, rate of convergence, length of the period, and sign pattern of consecutive corrections. The part of the perturbation that causes slow convergence and divergence can then be identified which may assist in the development of improved perturbation methods.

The organization of the paper is as follows. In Sec. II, we give a brief review of the criteria of convergence for perturbation expansions in a finite dimensional space. This is followed in Sec. III by the introduction of the two-state model for symmetric and asymmetric perturbations, a discussion of the criterion for convergence in this model, and the analytic expression for the energy-corrections of general order. In Sec. IV, we start the analysis of specific forms of archetypes by considering the two extreme cases where the size of the gap-shift is either much smaller or much larger than the size of the coupling term, giving the zigzag and geometric archetypes, respectively. In order to proceed beyond these extremes, we consider in Sec. V the functional form of the corrections in more detail and develop simple geometric progressions that have the same overall behavior as the full corrections. This also allows the determination of rates of convergence for symmetric as well as asymmetric perturbations. In Sec. VI, the perturbation expansions are considered in more detail for symmetric perturbations, and three additional archetypes, interspersed zigzag, triadic, and ripples, are introduced and analyzed. In Sec. VII, we perform a similar analysis for asymmetric perturbations and introduce the two remaining archetypes, zigzag-geometric, and convex-geometric. In Sec. VIII, we analyze several perturbation expansions and show how they fit into our classification scheme and how the numerical values of the higher order corrections can be used to identify the parameters of the two-state perturbation. Finally, in Sec. IX, we summarize and perspectivize our findings.

## II. CONVERGENCE OF PERTURBATION EXPANSIONS

To put the question of convergence or divergence of a perturbation expansion in a mathematical setting, we introduce a perturbation strength  $z$  and matrix representation of the perturbation expansion

$$\mathbf{H}(z) = \mathbf{H}_0 + z\mathbf{V}, \quad (1)$$

where  $\mathbf{H}_0$  and  $\mathbf{V}$  are the zeroth-order Hamiltonian and perturbation, respectively. The physical Hamiltonian for the system of interest is  $\mathbf{H}(1)$ . As we are interested in the question of convergence of perturbation expansions as they occur in actual calculations, the dimension of the expansion is finite. We will furthermore restrict it to the consideration of real matrices  $\mathbf{H}_0$ ,  $\mathbf{V}$ . Specifically, we are

interested in determining a selected root, typically the ground state, of the eigenvalue problem

$$\mathbf{H}(z)\mathbf{C}(z) = E(z)\mathbf{C}(z) \quad (2)$$

and wish to determine the values of  $z$  for which  $E(z)$  is an analytic function, so the Taylor or power-series expansion of  $E(z)$  converges to  $E(z)$ . Rellich showed<sup>7</sup> that  $E(z)$  is analytic in the region around 0 that does not contain a critical point, i.e., a value of  $z$  for which the eigenvalue of interest becomes degenerate. Denoting the critical point with the lowest norm  $|z|$  as the primary critical point, the perturbation expansion of the eigenvalue  $E(1)$  is convergent if the primary critical point is outside the complex unit-circle.

If a critical point is within the unit-circle, the additional state giving rise to the degeneracy is termed an intruder state, and the intruder state associated with a primary critical point is the primary intruder state. An intruder state associated with a critical point that has a negative real value of  $z$  is a back-door intruder, whereas a positive real value leads to a front-door intruder.

The primary critical point is of special interest as it determines the convergence radius of the perturbation expansion of  $E(z)$ . The primary critical point may be identified without the use of complex arithmetic by scanning the spectrum of  $E(z)$  as a function of real  $z$  and determine the avoided crossing with the lowest absolute value of  $z$ . The two states comprising this avoided crossing define a two-dimensional space. The zeroth-order Hamiltonian and the perturbation are then calculated in this two-dimensional space, and the critical values of  $z$  for this two-dimensional problem are determined and used as an approximation to the primary critical point of the full eigenvalue problem. If the imaginary part of the critical  $z$  is small, the above procedure reproduces critical points with high accuracy, but the approach may otherwise have a significant error.

For the MPPT series, it has been shown that the primary critical point may be obtained from the vector that defines the higher-order corrections to the wave function.<sup>21</sup> It has also been demonstrated that the two states that determines the avoided crossing with the lowest values of  $|z|$  may be used to identify the convergence rate and the higher-order corrections.<sup>21</sup> For MPPT series, there exists thus a fundamental and nontrivial relation between the primary intruder state and the higher-order corrections. In the present paper, it is demonstrated that the convergence rate and pattern of the higher order corrections of the CCPT and CP series may also be obtained from the perturbation expansion in a two-dimensional space spanned by the two states of the first avoided crossing.

In the above discussion, we considered a perturbation expansion of a Hermitian eigenvalue equation. In coupled cluster theory, a set of nonlinear equations is expanded in the perturbation and the convergence behavior then becomes connected with the properties of the non-Hermitian Jacobian as a function of the perturbation strength, rather than the Hamiltonian matrix *per se*.<sup>15</sup> Convergence of the perturbation expansion of the ground state energy is ensured if the Jacobian does not have any singularities for complex perturbation strengths within the complex unit circle.<sup>15</sup> The convergence behavior of these expansions can again be understood in terms of two states: the ground-state and the lowest excited state obtained

from the Jacobian; both are obtained at the perturbation strength of the first avoided crossing. For coupled cluster perturbation expansions of a given excitation energy, the convergence of the perturbation expansion is also defined by the Jacobian, with the additional convergence criterion that the excitation energy obtained as an eigenvalue of the perturbation dependent Jacobian does not have any degeneracy for perturbation strengths within the unit-circle.<sup>18</sup> Assuming that the perturbation expansion of the ground-state is converging, the convergence of the perturbation expansion of an excitation energy can thus be understood in terms of the energies and interactions of the excitations to the two states comprising the first avoided crossing of the excitation energy curve as a function of the perturbation strength. As the Jacobian is a nonsymmetric matrix, the two-state model has to be extended to consider a nonsymmetric Hamiltonian to describe these series.

### III. THE TWO-STATE HAMILTONIAN

We consider a real general two-state Hamiltonian  $\mathbf{H}$  and choose a basis, where the zeroth-order Hamiltonian  $\mathbf{H}_0$  is diagonal

$$\mathbf{H} = \mathbf{H}_0 + \mathbf{V}, \quad (3)$$

$$\mathbf{H}_0 = \begin{pmatrix} \alpha & 0 \\ 0 & \beta + \gamma \end{pmatrix}, \quad (4)$$

$$\mathbf{V} = \begin{pmatrix} 0 & \delta_2 \\ \delta_1 & -\gamma \end{pmatrix}. \quad (5)$$

The diagonal terms  $\alpha$  and  $\beta + \gamma$  are the zeroth-order energies of the reference and the additional state, respectively,  $\gamma$  is the gap-shift, and  $\delta_1, \delta_2$  are the coupling terms between the two states. All these parameters are assumed real. Note that the perturbation is not assumed to be Hermitian. In the following, we will use the assumption of non-degeneracy to require that the states have been ordered so  $\alpha < \beta + \gamma$ , so the first state has the lowest zeroth-order energy of the two states. We will also for convenience assume that  $\alpha < \beta$ , so the numerical ordering of the diagonal does not change in the interval  $z \in [0, 1]$ . However, most of the general features in the following, in particular, the types and forms of archetypes, does not depend on this assumption.

#### A. Eigenvalues

The eigenvalues of the matrix  $\mathbf{H}_0 + z\mathbf{V}$  are the solutions to the equation  $\det(\mathbf{H}_0 + z\mathbf{V} - E\mathbf{1}) = 0$ , which leads to the identifications

$$E_{\pm}(z) = \frac{\alpha + \beta + (1-z)\gamma}{2} \pm \frac{\sqrt{(\alpha - \beta - (1-z)\gamma)^2 + 4\delta_1\delta_2z^2}}{2}. \quad (6)$$

It is noted that the eigenvalues for an arbitrary value of  $z$  depend on the product  $\delta_1\delta_2$  and not on the individual values of  $\delta_1$  and  $\delta_2$ . Introducing a geometrically averaged non-negative coupling term  $\delta$  and a symmetry factor  $\sigma$ ,

$$\delta_1\delta_2 = \sigma\delta^2, \quad \sigma = \begin{cases} +1 & \text{if } \delta_1\delta_2 \geq 0, \\ -1 & \text{if } \delta_1\delta_2 < 0, \end{cases} \quad (7)$$

and the eigenvalues of Eq. (6) may be written as

$$E_{\pm}(z) = \frac{\alpha + \beta + (1-z)\gamma}{2} \pm \frac{\sqrt{(\alpha - \beta - (1-z)\gamma)^2 + 4\sigma\delta^2z^2}}{2}. \quad (8)$$

The perturbation with  $\sigma = 1$  will be denoted a symmetric perturbation, whereas a perturbation with  $\sigma = -1$  is an asymmetric perturbation.

The eigenvalues  $E_{\pm} = E_{\pm}(1)$  according to Eq. (8) are given as

$$E_{\pm} = \frac{\alpha + \beta}{2} \pm \frac{\sqrt{(\alpha - \beta)^2 + 4\sigma\delta^2}}{2}. \quad (9)$$

The relations between the eigenvalues  $E_{\pm}$  and the diagonal elements of  $\mathbf{H} = \mathbf{H}(1)$  depend on the symmetry factor. Since the square root is a monotonically increasing function, it is first noted that  $\sqrt{(\alpha - \beta)^2 + 4\sigma\delta^2}$  is larger than  $\beta - \alpha$  for  $\sigma = 1$  and smaller than  $\beta - \alpha$  for  $\sigma = -1$ . The symmetric perturbation problem for real  $z$  therefore has a lowest eigenvalue,  $E_-$ , that is below  $\alpha$  and a largest eigenvalue,  $E_+$ , that is above  $\beta$ . For an asymmetric perturbation and  $\delta < \frac{\beta - \alpha}{2}$ , one obtains a real lowest eigenvalue that for real  $z$  is larger than  $\alpha$  and a real largest eigenvalue that is lower than  $\beta$ , whereas the eigenvalues for  $\delta > \frac{|\beta - \alpha|}{2}$  become a pair of complex conjugated numbers

$$E_{\pm} = \frac{\alpha + \beta}{2} \pm \frac{\sqrt{4\delta^2 - (\alpha - \beta)^2}}{2}, \quad i, \sigma = -1, \delta > \frac{\beta - \alpha}{2}. \quad (10)$$

If  $\delta = \frac{|\beta - \alpha|}{2}$ , the eigenvalues of the asymmetric problem become degenerate. A general two-dimensional matrix may be defective, i.e., have only a one-dimensional space of eigenvectors. In Appendix A, it is shown that a general two-dimensional matrix is defective if and only if the two eigenvalues are degenerate and at least one of the off-diagonal matrix elements is nonvanishing. The use of the word degenerate to describe the case where the two eigenvalues are identical does therefore here not imply that there are two linearly independent eigenvectors.

#### B. General expressions for the energy-corrections in the two-state model

The perturbation expansion of Eq. (8) in Ref. 21 was considered for a symmetric perturbation. This treatment may be generalized to include the asymmetric perturbation, and one obtains the energy-corrections  $E^{(n)}$  of the lowest state for a general order  $n$  as

$$\begin{aligned} E^{(0)} &= \alpha, \\ E^{(1)} &= 0, \\ E^{(n)} &= \frac{\gamma^n}{(\beta + \gamma - \alpha)^{n-1}} e^{(n)}\left(\sigma, \left|\frac{\delta}{\gamma}\right|\right), \quad n > 1, \end{aligned} \quad (11)$$

where

$$e^{(n)}\left(\sigma, \left|\frac{\delta}{\gamma}\right|\right) = \sum_{i=1}^{[n/2]} e_i^{(n)}\left(\sigma, \left|\frac{\delta}{\gamma}\right|\right), \quad (12)$$

$$e_i^{(n)}\left(\sigma, \left|\frac{\delta}{\gamma}\right|\right) = (-\sigma)^i f_i^{(n)}\left(\frac{\delta}{\gamma}\right)^{2i}, \quad (13)$$

$$f_i^{(n)} = \frac{(n-2)!}{(n-2i)!i!(i-1)!}. \quad (14)$$

In Eq. (12),  $[n/2]$  is the largest integer not exceeding  $\frac{n}{2}$ . The energy-correction  $E^{(n)}$  is the product of the prefactor,  $\frac{\gamma^n}{(\beta+\gamma-\alpha)^{n-1}}$ , and a factor,  $e^{(n)}$ , which depends on the symmetry factor and the absolute value of the ratio between the coupling parameter and the gap-shift. The prefactor is a simple geometric series in  $n$ , whereas  $e^{(n)}$  gives rise to a number of patterns in the perturbation expansions and is examined in Sections V and VI. The signs of the corrections will also show a number of patterns, arising from rather complicated sign-changes of  $e^{(n)}$  and the signs of the prefactors, which for nonvanishing  $\gamma$  have the simple form

$$\text{sign}\left(\frac{\gamma^n}{(\beta+\gamma-\alpha)^{n-1}}\right) = (\text{sign}(\gamma))^n. \quad (15)$$

For  $\gamma = 0$ , the energy-corrections are straightforwardly obtained in the closed form by expanding the energy in Eq. (8) in  $z^2$  and are equal to the values obtained by taking limit  $\gamma \rightarrow 0$  in Eq. (11),

$$E^{(2n+1)} = 0, \quad (16)$$

$$\begin{aligned} E^{(2n)} &= (-\sigma)^n \frac{\delta^{2n}}{(\beta-\alpha)^{2n-1}} f_n^{(2n)} \\ &= (-\sigma)^n \frac{(2n-2)! \delta^{2n}}{n!(n-1)!(\beta-\alpha)^{2n-1}}. \end{aligned}$$

### C. Points of degeneracy for the energy function and radii of convergence

To examine whether the expansion in  $z$  of the eigenvalues  $E_{\pm} = E_{\pm}(1)$  is convergent or divergent, we determine, in accordance with the discussion of Sec. II, the complex values  $z^c$  where the two eigenvalues are degenerate,  $E_-(z^c) = E_+(z^c)$ . As mentioned above and shown in Appendix A, a two-dimensional matrix with degenerate eigenvalues is defective unless both off-diagonal elements are zero. Except for a trivial perturbation with vanishing coupling elements, the values  $z_c$  may alternatively be characterized as the values where the matrix  $\mathbf{H}(z)$  becomes defective. To identify  $z^c$ , we express the term inside the square-root of Eq. (8) as a second-order polynomial in  $z$ ,

$$\begin{aligned} (\alpha - \beta - (1-z)\gamma)^2 + 4\sigma\delta^2 z^2 &= (4\sigma\delta^2 + \gamma^2)z^2 + 2\gamma(\alpha - \beta - \gamma)z \\ &\quad + (\alpha - \beta - \gamma)^2. \end{aligned} \quad (17)$$

The critical points are the values of  $z$  for which the polynomial in Eq. (17) vanishes. For  $4\sigma\delta^2 + \gamma^2 = 0$ , there is a single critical point

$$z^c = \frac{\beta - \alpha + \gamma}{2\gamma}, \quad 4\sigma\delta^2 + \gamma^2 = 0, \quad (18)$$

whereas a nonvanishing value of  $4\sigma\delta^2 + \gamma^2$  leads to a pair of critical points

$$z_{\pm}^c = \frac{\beta - \alpha + \gamma}{4\sigma\delta^2 + \gamma^2} (\gamma \pm 2\sqrt{-\sigma\delta^2}), \quad 4\sigma\delta^2 + \gamma^2 \neq 0. \quad (19)$$

For a symmetric perturbation, the critical points of Eq. (19) become a pair of complex conjugated numbers

$$z_{\pm}^c = \frac{\beta - \alpha + \gamma}{4\delta^2 + \gamma^2} (\gamma \pm 2\delta i), \quad \sigma = +1, \quad (20)$$

and the common norm of the critical points is

$$|z_{\pm}^c| = \frac{\beta - \alpha + \gamma}{\sqrt{4\delta^2 + \gamma^2}}, \quad \sigma = 1. \quad (21)$$

The perturbation expansion is absolutely convergent if  $|z_{\pm}^c| > 1$  and divergent if  $|z_{\pm}^c| < 1$ . If  $|z_{\pm}^c| = 1$ , a thorough analysis is needed to determine whether the expansion is convergent or divergent. As it is unlikely that the condition  $|z_{\pm}^c| = 1$  will be observed in any actual calculations, such an analysis will not be attempted here. The condition for divergence from Eq. (21) is seen to correspond to

$$\text{sign}(\beta - \alpha)\gamma < \frac{|\beta - \alpha|}{2} \left( \left( \frac{2\delta}{\beta - \alpha} \right)^2 - 1 \right) \Leftrightarrow |z_{\pm}^c| < 1, \quad \sigma = 1. \quad (22)$$

From Eq. (22), it follows for  $\beta - \alpha > 0$  that

$$\gamma < \gamma_c = -\frac{\beta - \alpha}{2} \Rightarrow |z_{\pm}^c| < 1. \quad (23)$$

There exists thus a critical value  $\gamma_c = -\frac{\beta - \alpha}{2}$  for which the expansions are divergent for  $\gamma < \gamma_c$  for all values of  $\delta$ .

From Eq. (20), it is seen that a positive value of the gap-shift gives a pair of critical points in the half-plane with positive real values of  $z_{\pm}$ , whereas a negative value of the gap-shift gives critical points in the negative half-plane. Intruder states corresponding to a positive or negative value of gap-shift are thus front door or back door intruder states, respectively. It is also noted that the argument (the angle between a point in the complex plane and the positive real axis) of each of the points of degeneracy depends only on the relative magnitude of the gap-shift and the coupling element. If the gap-shift is much larger than the coupling element, the points of degeneracy are close to the real axis, whereas a gap-shift that is much smaller than the coupling element leads to points of degeneracy that are close to the imaginary axis.

For an asymmetric perturbation, we first assume that  $-4\delta^2 + \gamma^2 \neq 0$  so the critical points of Eq. (19) become two points in the real axis

$$z_{\pm}^c = \frac{\beta - \alpha + \gamma}{\gamma \mp 2\delta}, \quad \sigma = -1, \quad -4\delta^2 + \gamma^2 \neq 0. \quad (24)$$

The radius of convergence is given by  $\min(|z_-^c|, |z_+^c|)$ . Since  $|\gamma - 2\delta| > |\gamma + 2\delta|$  for negative values of  $\gamma$  and  $|\gamma - 2\delta| < |\gamma + 2\delta|$  for positive values of  $\gamma$ , we have

$$\min(|z_-^c|, |z_+^c|) = \frac{\beta - \alpha + \gamma}{|2\text{sign}(\gamma)\delta + \gamma|}. \quad (25)$$

By writing  $\gamma$  as  $\text{sign}(\gamma)|\gamma|$ , we may rewrite Eq. (25) as

$$\min(|z_-^c|, |z_+^c|) = \frac{\beta - \alpha + \gamma}{|2\text{sign}(\gamma)\delta + \text{sign}(\gamma)|\gamma|} = \frac{\beta - \alpha + \gamma}{2\delta + |\gamma|}. \quad (26)$$

For  $-4\delta^2 + \gamma^2 = (\gamma + 2\delta)(\gamma - 2\delta) = 0$ , the critical point of Eq. (18) equals either  $z_-^c$  or  $z_+^c$  of Eq. (24), whereas the other value of  $z_{\pm}^c$  in Eq. (24) becomes infinite. Equation (26) holds therefore for all values of  $\gamma$  and  $\delta$ .

To determine a critical value  $\gamma_c$  of  $\gamma$ , we identify the values of  $\gamma$  for which

$$\frac{\beta - \alpha + \gamma}{2\delta + |\gamma|} < 1 \quad (27)$$

holds for all values of  $\delta$ . For positive values of  $\gamma$ , it is noted that Eq. (27) is not fulfilled for  $\delta = 0$ , so critical values of  $\gamma$  must be nonpositive. For nonpositive values of  $\gamma$ , the divergence criterion of Eq. (27) becomes

$$\gamma < -\frac{\beta - \alpha}{2} + \delta, \quad (28)$$

so the expansion is divergent for all (positive) values of  $\delta$  if  $\gamma < -\frac{\beta - \alpha}{2}$ . The critical value of  $\gamma$  is therefore also given by Eq. (23) for asymmetric perturbations.

#### IV. ONE-TERM APPROXIMATIONS

In general, several terms contribute to  $e^{(n)}$  in Eq. (11), but there are two limiting cases where a single term dominates:  $|\gamma| \ll |\delta|$  and  $|\gamma| \gg |\delta|$ . These two cases give the first archetypes of convergence: the zigzag and geometric patterns. We will now consider these cases, starting with  $\gamma = 0$ , which may be considered as a special case of  $|\gamma| \ll |\delta|$ . For the mathematical analysis, we continue the use of general values of  $\alpha$ ,  $\beta$ ,  $\gamma$ , and  $\delta$ , but for the numerical evaluations, we use the value  $\beta - \alpha = 1$ , which corresponds to the use of the scaled gap-shift and coupling,  $\gamma_s$ ,  $\delta_s$ , defined as

$$\begin{aligned} \gamma_s &= \frac{\gamma}{\beta - \alpha}, \\ \delta_s &= \frac{\delta}{\beta - \alpha}. \end{aligned} \quad (29)$$

##### A. $\gamma = 0$

For  $\gamma = 0$ , it follows from Eq. (22) for a symmetric perturbation and from Eq. (28) for an asymmetric perturbation that the expansion is convergent if

$$\delta < \frac{\beta - \alpha}{2}. \quad (30)$$

The corrections in Eq. (16) shows that the corrections vanish for odd values of  $n$  and reduce to a single term for even  $n$ , which may be rewritten using the double factorial defined as  $(2n - 3)!! = (2n - 3)(2n - 5)\dots 1$ ,

$$E^{(2n+1)} = 0, \quad (31)$$

$$\begin{aligned} E^{(2n)} &= (-\sigma)^n \frac{\delta^{2n}}{(\beta - \alpha)^{2n-1}} f_n^{(2n)} = (-\sigma)^n \frac{(2n - 2)!}{n!(n - 1)!} \frac{\delta^{2n}}{(\beta - \alpha)^{2n-1}} \\ &= (-\sigma)^n \frac{(2n - 3)!! 2^{n-1}}{n!} \frac{\delta^{2n}}{(\beta - \alpha)^{2n-1}}. \end{aligned}$$

For symmetric perturbations, the even orders have alternating signs with  $E^{(2n)}$  being positive for even values of  $n$  and negative for odd values of  $n$ . For an asymmetric perturbation, all even corrections are positive.

The deviation (error) of the energy calculated through order  $k$  and the eigenvalue  $E_-$  is defined as

$$D_k = \sum_{i=0}^k E^{(i)} - E_-(1). \quad (32)$$

In Appendix B, it is shown that the remainder for  $\gamma = 0$  becomes

$$\begin{aligned} D_{2n} = D_{2n+1} &= \frac{\sigma(-\sigma)^n (2n - 1)!! 2^n}{(n + 1)!} \frac{\delta^{2n+2}}{(\beta - \alpha)^{2n+1}} \\ &\times \sqrt{1 + \frac{4\sigma\delta^2}{(\beta - \alpha)^2}} \xi, \quad \xi \in [0, 1]. \end{aligned} \quad (33)$$

We can now compare the signs of the corrections  $E^{(2n)}$  of Eq. (31) with the signs of the deviations  $D_{2n}$  in Eq. (33). For a symmetric perturbation, the corrections and deviations have identical signs at each order. This pattern is seen in left panels of Fig. 1 which gives the perturbation corrections and deviations for symmetric perturbations with  $\delta = 0.4$  for three values of  $\gamma$ , including  $\gamma = 0$ .

For an asymmetric perturbation, it is seen from Eq. (33) that all deviations are negative, whereas the corrections were found to be positive. In this case, the converged eigenvalue is approached systematically from below. This behavior is also observed in the right panels of Fig. 1 that contains the corrections and deviations for an asymmetric perturbation with  $\delta = 0.4$  and the three values of  $\gamma$  including zero.

##### B. The zigzag archetype: $|\gamma| \ll |\delta|$

We next consider a nonvanishing gap-shift that is numerically much smaller than the coupling and restrict us to orders that are so low that only the term in Eq. (11) of lowest order in  $\gamma$  contributes noticeably to the energy-corrections. We will later (Sec. VI A) return to an analysis of the orders for which this approximation holds. It is thus assumed that the only term that contributes significantly to  $e^{(n)}$  in Eq. (12) is the term  $e_{[\frac{n}{2}]}^{(n)}$  and we obtain for even  $n$ ,

$$\begin{aligned} e^{(n)} &\approx e_{[\frac{n}{2}]}^{(n)} = (-\sigma)^{\frac{n}{2}} \frac{(n - 2)!}{\frac{n}{2}!(\frac{n}{2} - 1)!} \left| \frac{\delta}{\gamma} \right|^n, \\ e^{(n+1)} &\approx e_{[\frac{n}{2}]}^{(n+1)} = (-\sigma)^{\frac{n}{2}} \frac{(n - 1)!}{(\frac{n}{2})!(\frac{n-2}{2})!} \left| \frac{\delta}{\gamma} \right|^n. \end{aligned} \quad (34)$$

The energy corrections become

$$\begin{aligned} E^{(n)} &\approx \frac{\gamma^n}{(\beta + \gamma - \alpha)^{n-1}} e_{[\frac{n}{2}]}^{(n)} = (-\sigma)^{\frac{n}{2}} \frac{(n - 2)!}{\frac{n}{2}!(\frac{n}{2} - 1)!} \frac{\delta^n}{(\beta + \gamma - \alpha)^{n-1}}, \\ E^{(n+1)} &\approx \frac{\gamma^{n+1}}{(\beta + \gamma - \alpha)^n} e_{[\frac{n}{2}]}^{(n+1)} = (-\sigma)^{\frac{n}{2}} \frac{(n - 1)!}{\frac{n}{2}!(\frac{n}{2} - 1)!} \frac{\gamma\delta^n}{(\beta + \gamma - \alpha)^n}, \end{aligned} \quad (35)$$

where we have used that  $\frac{\gamma^n}{|\gamma|^n} = 1$  since  $n$  is even. The absolute ratio between an odd- and the preceding even-order corrections is from the above equations obtained as

$$\left| \frac{E^{(n+1)}}{E^{(n)}} \right| = \frac{(n - 1)|\gamma|}{\beta + \gamma - \alpha}, \quad (36)$$

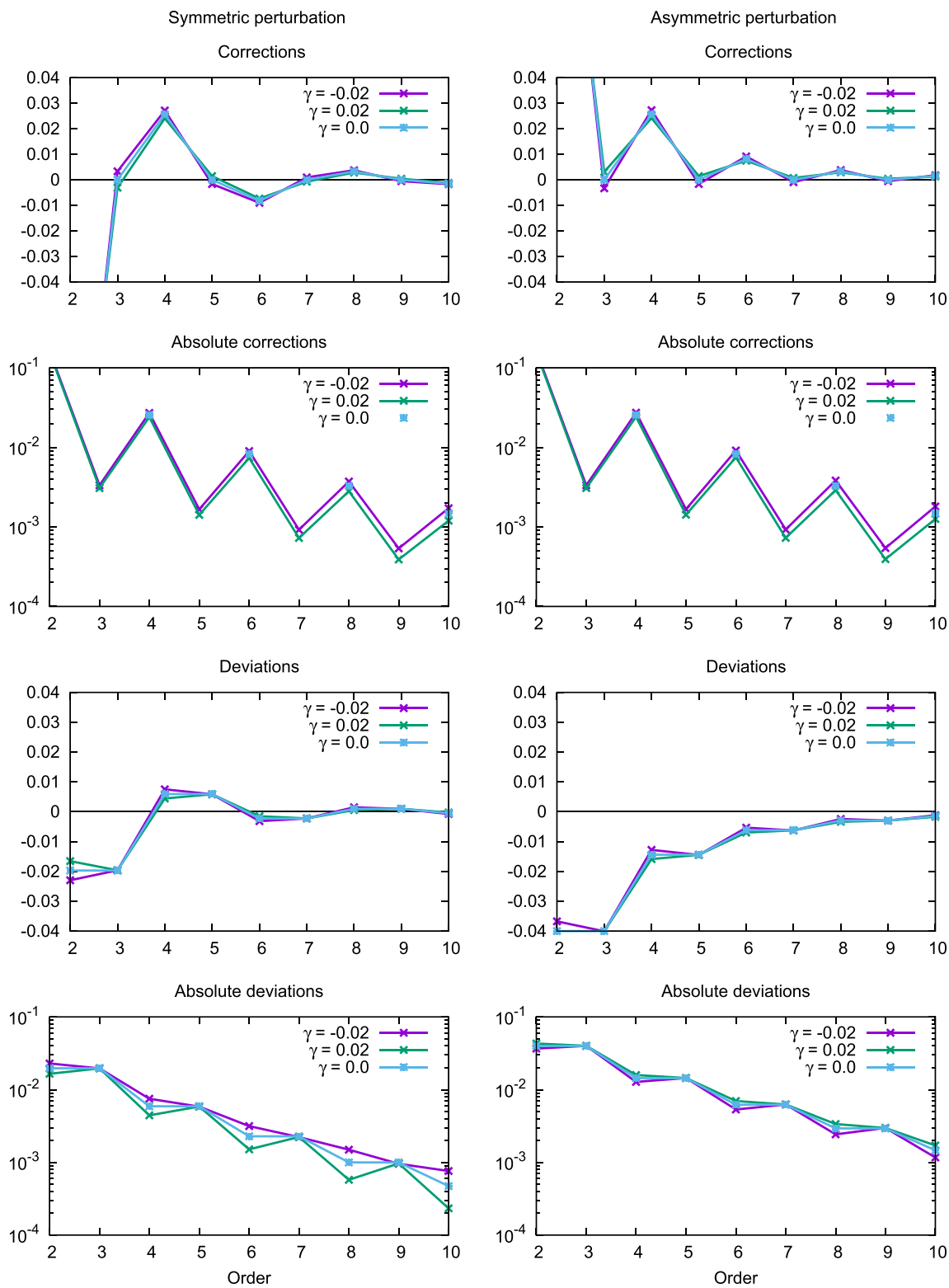


FIG. 1. Corrections and deviations for vanishing and very small gap-shifts and a coupling constant of 0.4 for a symmetric (left) and asymmetric (right) perturbation.



where the assumption  $\beta + \gamma - \alpha > 0$  has been used. The absolute ratio between an even- and the preceding odd-order corrections is similarly obtained as

$$\left| \frac{E^{(n+2)}}{E^{(n+1)}} \right| = \frac{4|\gamma|}{(n+2)(\beta + \gamma - \alpha)} \left( \frac{\delta}{\gamma} \right)^2. \quad (37)$$

Since  $\left| \frac{\delta}{\gamma} \right|$  by assumption is much larger than one, we see from Eqs. (36) and (37) for low orders that the size of the corrections change much more when going from an odd to the following even order correction than when going from an even to the following odd order. The curve of absolute corrections exhibits thus a zigzag pattern, so the archetype for  $\left| \frac{\delta}{\gamma} \right| \gg 1$  and lower orders  $n$  is denoted the zigzag archetype.

To obtain the pattern of the sign-corrections for a symmetric perturbation, it is noted from Eq. (34) that the signs of  $e^{(n)}$  and  $e^{(n+1)}$  for  $n$  even are equal to  $(-1)^{\frac{n}{2}}$  and depend therefore on whether the even number  $n$  divided by 2 is even or odd. The signs of  $e^{(n)}$  will therefore exhibit a period of four. For an arbitrary  $k$  and  $i \in [0, 3]$ , we obtain from Eq. (34) that the signs of  $e^{(4k+i)}$  are 1, 1, -1, -1 for  $i = 0, 1, 2, 3$ . From Eq. (35), it is seen that the sign of the correction  $E^{(n)}$  equals the sign of  $\gamma^n$  times the sign of  $e^{(n)}$  for arbitrary (even or odd) values of  $n$ . For a negative value of the gap-shift, the signs of  $E^{(4k+i)}$  for  $i = 0, 1, 2, 3$  become therefore  $(1 \times 1, -1 \times 1, 1 \times -1, -1 \times -1) = (1, -1, -1, 1)$ , whereas the signs of  $E^{(4k+i)}$  for a positive gap-shift are  $(1, 1, -1, -1)$ . Connecting several of these sign-patterns of period 4, we see that the sign-pattern becomes  $(2-, 2+)$  for both a negative gap-shift and a positive gap-shift.

For an asymmetric Hamiltonian, it is seen from Eq. (34) that  $e^{(n)}$  is positive for all orders, so the even-ordered corrections are all positive, whereas the sign of the odd corrections equals the sign of the gap-shift. A positive gap-shift leads thus to positive corrections, and a negative gap-shift leads to the  $(1+, 1-)$  pattern with the even corrections being positive.

The convergence behavior for small gap-shifts and a symmetric perturbation is illustrated in the left panels of Fig. 1, which contains the corrections, absolute corrections, deviations, and absolute deviations for  $\delta = 0.4$  and  $\gamma = \pm 0.02$  and 0. The absolute corrections exhibit the expected zigzag pattern, and their behavior is in agreement with the above analysis. The right panels of Fig. 1 give the same information for an asymmetric perturbation and the above values of  $\delta$  and  $\gamma$ . All even corrections are positive, whereas the odd corrections are negative for the negative gap-shift and positive for the positive gap-shift. For all the considered choices of  $\gamma$ , the deviations are negative.

A summary of the convergence patterns for the zigzag archetype is given in the left column of Table I. A logarithmic plot is used to allow plotting over a large range of function values. To ensure information about the signs in the logarithmic plot, we introduce a simple color coding of a given function value: a red circle corresponds to a negative function value, whereas a blue cross corresponds to a positive function value. The absolute size of an even correction is significantly larger than the size of both the preceding and the following odd order correction. For a symmetric perturbation, both the corrections and deviations show a  $(2+, 2-)$  behavior for both signs of  $\gamma$ . For asymmetric perturbations and a positive

gap-shift, all corrections in Table I are positive and all deviations are negative. If the gap-shift is negative, one obtains the pattern  $(1+, 1-)$  for the corrections with the even order corrections being positive, whereas the deviations are all negative. For an asymmetric perturbation, the converged energy is thus approached monotonically from below.

### C. Geometric expansions: $|\gamma| \gg |\delta|$

The second case where a single term dominates the energy corrections occurs when the size of the gap-shift is much larger than the size of the coupling. For sufficiently small orders,  $e^{(n)}$  in Eq. (12) is then dominated by the term  $e_1^{(n)}$ , so we may write

$$e^{(n)} \approx e_1^{(n)} = -\sigma \frac{\delta^2}{\gamma^2}, \gamma \gg \delta. \quad (38)$$

In this one-term model, the energy corrections and rate of convergence become<sup>21</sup>

$$E^{(n)} = -\sigma \frac{\delta^2 \gamma^{n-2}}{(\beta + \gamma - \alpha)^{n-1}}, \quad (39)$$

$$r = \left| \frac{E^{(n+1)}}{E^{(n)}} \right| = \frac{|\gamma|}{\beta + \gamma - \alpha}.$$

This one-term model has previously been used to analyze and explain the convergence behavior as well as signs of corrections occurring in MPPT for very small coupling constants.<sup>21</sup> In the one-term model defined by Eq. (39), the energy corrections follow a simple geometric progression and we therefore denote this archetype as the geometric archetype. The sign pattern of the corrections is given by the signs of  $-\sigma \gamma^{n-2}$ . For a symmetric perturbation, the sign patterns are thus  $(1-)$  for a positive gap-shift, where we use the notation  $(1-)$  for the signs of a series that only contains negative corrections. For a negative gap-shift, the sign pattern is  $(1+, 1-)$  with the even orders being negative. For an asymmetric perturbation, the sign patterns are opposite to that of the symmetric perturbation, so a positive gap-shift gives the sign pattern  $(1+)$  and a negative gap-shift gives the pattern  $(1+, 1-)$  with the even order corrections being positive.

Examples of corrections for  $\gamma \gg \delta$  are given in the upper parts of the second column of Table I for symmetric perturbations and for asymmetric perturbations in the lower parts of the column. The parameters  $\gamma = \pm 0.4$ ,  $\delta = 0.008$  are used for both forms of perturbations to illustrate the behavior for positive and negative gap-shifts. For each set of values of  $\gamma$  and  $\delta$ , the size of the corrections is identical for a symmetric and asymmetric, whereas the sign patterns in agreement with the above analysis are different.

A summary of the convergence patterns for the geometric archetype is given in the right column of Table I. For both symmetric and asymmetric perturbations, the sizes of the absolute corrections and deviations follow a simple geometric progression. For a symmetric perturbation, a positive gap-shift leads to negative corrections and positive deviations, whereas a negative gap-shift leads to alternating signs, i.e., the  $(1+, 1-)$  sign pattern, for corrections and deviations. For an asymmetric perturbation, a positive gap-shift gives positive corrections and negative deviations, whereas a negative gap-shift leads to the  $(1+, 1-)$  sign pattern for corrections and deviations.

TABLE I. The one-term archetypes for symmetric and asymmetric perturbations.

Type	Zigzag	Geometric	
Identification	$ \gamma  \ll  \delta $	$ \gamma  \gg  \delta $	
Symmetric perturbation, rate of convergence: $\frac{\sqrt{4\delta^2 + \gamma^2}}{\beta + \gamma - \alpha}$			
Typical form of corrections and deviations			
Asymmetric perturbation, rate of convergence: $\frac{2\delta +  \gamma }{\beta + \gamma - \alpha}$			
Typical form of corrections and deviations			

## V. A CLOSER EXAMINATION OF THE FUNCTIONS $e^{(n)}(\sigma, \left|\frac{\delta}{\gamma}\right|)$

To understand the behavior of the energy corrections beyond the simple one-term models of Sec. IV C, it is necessary to examine the functions  $e^{(n)}(\sigma, \left|\frac{\delta}{\gamma}\right|)$  of Eq. (13) in closer detail. We start the analysis of these functions in this section and provide a thorough analysis in Secs. VI and VII.

### A. Introduction to the functions $e^{(n)}$

The absolute values of  $e^{(n)}(+, \left|\frac{\delta}{\gamma}\right|)$  and  $e^{(n)}(-, \left|\frac{\delta}{\gamma}\right|)$  for  $\left|\frac{\delta}{\gamma}\right| = 0.02, 0.25, 0.4, 0.5, 1, 2, 10,$  and  $50$  are given for orders up to 100 in Figs. 2 and 3, respectively. The observed identity of the lowest orders of  $e^{(n)}$  follows directly from Eqs. (12) and (13),

$$e^{(2)}(\sigma, \left|\frac{\delta}{\gamma}\right|) = e^{(3)}(\sigma, \left|\frac{\delta}{\gamma}\right|) = -\sigma \left(\frac{\delta}{\gamma}\right)^2. \quad (40)$$

In general, the curves for  $|e^{(n)}(+, \left|\frac{\delta}{\gamma}\right|)|$  have a periodic structure with significant variance in the form as well as the length of the periods. For values of  $\left|\frac{\delta}{\gamma}\right|$  smaller than one, the curves have a periodic structure that we will describe as ripples. The periods of the ripples increase for decreasing values of  $\left|\frac{\delta}{\gamma}\right|$ . In each ripple, the sign is constant and the size  $|e^{(n)}(+, \left|\frac{\delta}{\gamma}\right|)|$  first increases and then decreases. The sign changes when going from one period to the next. For  $\left|\frac{\delta}{\gamma}\right| = 1$ , the curve has a dominant period of three. As  $\left|\frac{\delta}{\gamma}\right|$  increases beyond 1,  $e^{(n)}(+, \left|\frac{\delta}{\gamma}\right|)$  becomes a fast rising function of  $n$ , where small and

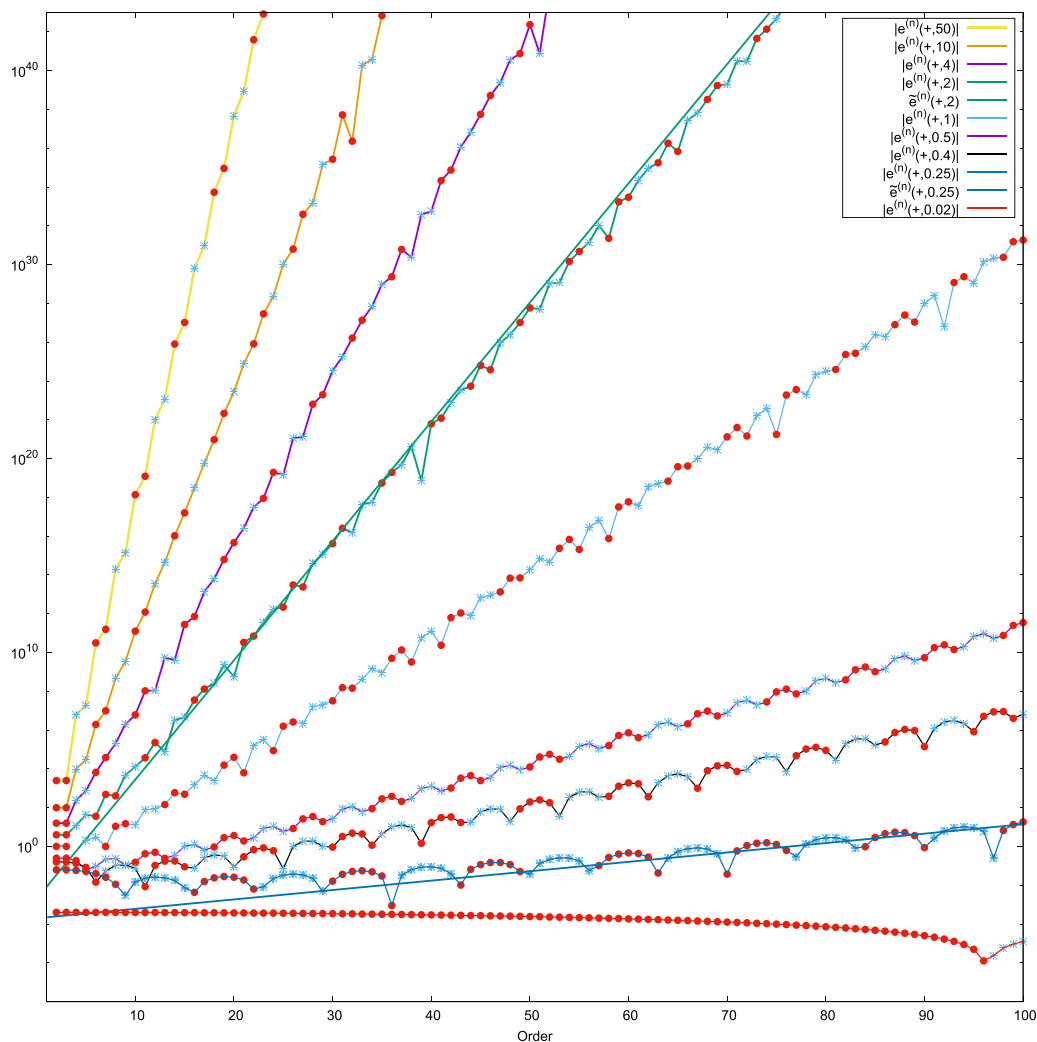


FIG. 2. Plot of  $|e^{(n)}(+, \left|\frac{\delta}{\gamma}\right|)|$  and  $\bar{e}^{(n)}(+, \left|\frac{\delta}{\gamma}\right|)$  up to order 100 for different values of  $\left|\frac{\delta}{\gamma}\right|$ .

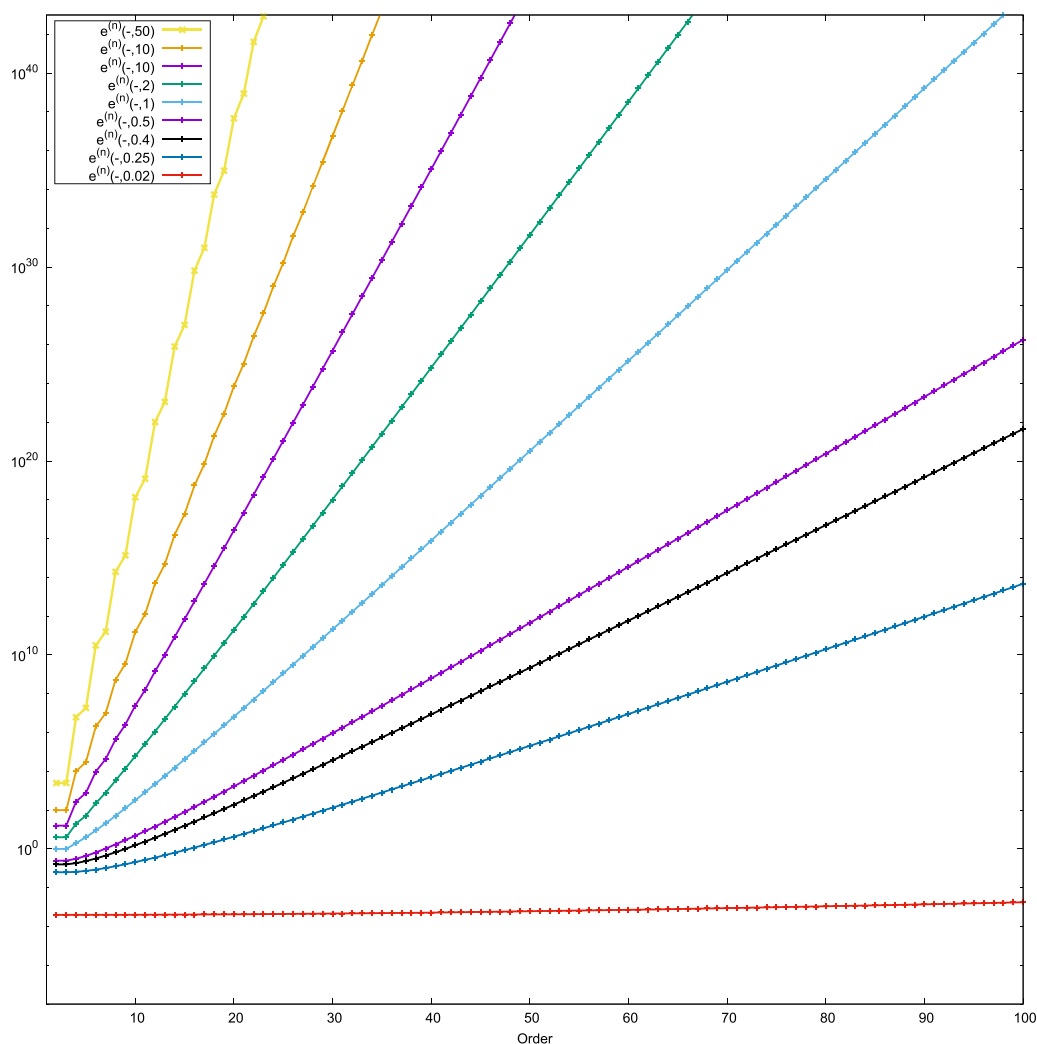


FIG. 3. Plot of  $e^{(n)}(-, |\frac{\delta}{\gamma}|)$  up to order 100 for different values of  $|\frac{\delta}{\gamma}|$ . Negative values are marked by red pluses and positive values by blue crosses.

large corrections follow each other for lower orders, and the (2+, 2-) sign pattern becomes dominating.

The periodic behavior of  $e^{(n)}(+, |\frac{\delta}{\gamma}|)$  outlined above and the changes of this behavior for increasing  $|\frac{\delta}{\gamma}|$  is important for the understanding of the patterns and periods of the perturbation corrections  $E^{(n)}$  in Eq. (11). We will in Sec. VI analyze this behavior using expansions of  $e^{(n)}$  that contains more than a single term.

We next consider the functions  $e^{(n)}(-, |\frac{\delta}{\gamma}|)$  in Fig. 3. For the limiting cases,  $|\gamma| \ll |\delta|$  and  $|\gamma| \gg |\delta|$ , exemplified in the figures by  $|\frac{\delta}{\gamma}| = 50$  and  $|\frac{\delta}{\gamma}| = 0.02$ , the curves for  $e^{(n)}(-, |\frac{\delta}{\gamma}|)$  in Fig. 3 and  $e^{(n)}(+, |\frac{\delta}{\gamma}|)$  in Fig. 2 are very similar. For values of  $|\frac{\delta}{\gamma}|$  closer to one, there are pronounced differences between  $e^{(n)}(-, |\frac{\delta}{\gamma}|)$  and  $e^{(n)}(+, |\frac{\delta}{\gamma}|)$ . In particular, for  $|\frac{\delta}{\gamma}|$  smaller than or equal to 10,

$e^{(n)}(-, |\frac{\delta}{\gamma}|)$  show a smooth and monotonic behavior at higher order without any recurring patterns.

## B. Geometric approximations to $e^{(n)}$ and $E^{(n)}$

In this section, we will develop a geometric approximation to  $|e^{(n)}(\sigma, |\frac{\delta}{\gamma}|)|$  as a function of  $n$ . The construction of a geometric approximation to  $|e^{(n)}(+, |\frac{\delta}{\gamma}|)|$  may seem problematic as it was seen in Fig. 2 that the functions may have a zigzag or ripple pattern. However, the figures also show that curves for  $|e^{(n)}(+, |\frac{\delta}{\gamma}|)|$  over many orders have a geometric convergence. For example, the local maxima of  $|e^{(n)}(+, |\frac{\delta}{\gamma}|)|$  for  $|\frac{\delta}{\gamma}| = 0.25$  form to good accuracy a geometric progression. We therefore introduce a rate of convergence that reflects the convergence behavior of the corrections over many orders

$$r = \lim_{n \rightarrow \infty} \left( \frac{|E^{(k+n)}|}{|E^{(n)}|} \right)^{1/n}. \quad (41)$$

The geometric approximation to  $|e^{(n)}(\sigma, |\frac{\delta}{\gamma}|)|$  is defined as

$$\tilde{e}^{(n)}(\sigma, |\frac{\delta}{\gamma}|) = c_0(\sigma, |\frac{\delta}{\gamma}|) p(\sigma, |\frac{\delta}{\gamma}|)^n. \quad (42)$$

Since the constant  $c_0(\sigma, |\frac{\delta}{\gamma}|)$  does not effect the rate of convergence, we focus on the determination of the geometric factor  $p(\sigma, |\frac{\delta}{\gamma}|)$ . This factor will be determined by requiring that geometric approximation to the absolute energy corrections,

$$\tilde{E}^{(n)} = \frac{|\gamma^n|}{(\beta + \gamma - \alpha)^{n-1}} \tilde{e}^{(n)}(\sigma, |\frac{\delta}{\gamma}|), \quad (43)$$

has a convergence rate equal to one when the radius of convergence of the energy-corrections  $E^{(n)}$  of Eq. (21) is one. We thus introduce the convergence rate for  $\tilde{E}^{(n)}$ ,

$$\tilde{r} = \left| \frac{\tilde{E}^{(n+1)}}{\tilde{E}^{(n)}} \right| = \frac{|\gamma|}{\beta + \gamma - \alpha} p(\sigma, |\frac{\delta}{\gamma}|), \quad (44)$$

and require that  $\tilde{r} = 1$  when the convergence radius for  $E^{(n)}$  equals 1,

$$\tilde{r} = 1 \text{ for } \min(|z_+^c|, |z_-^c|) = 1. \quad (45)$$

To proceed, one needs to separately consider symmetric and asymmetric perturbations. In Appendix C, we determine the constants  $p(\sigma, |\frac{\delta}{\gamma}|)$  as

$$\begin{aligned} p(+, |\frac{\delta}{\gamma}|) &= \sqrt{4(\frac{\delta}{\gamma})^2 + 1}, \\ p(-, |\frac{\delta}{\gamma}|) &= 2|\frac{\delta}{\gamma}| + 1, \end{aligned} \quad (46)$$

and the convergence rates

$$\tilde{r} = \begin{cases} \frac{\sqrt{4\delta^2 + \gamma^2}}{\beta + \gamma - \alpha} & \text{for } \sigma = 1, \\ \frac{2\delta + |\gamma|}{\beta + \gamma - \alpha} & \text{for } \sigma = -1. \end{cases} \quad (47)$$

Since  $\sqrt{4\delta^2 + \gamma^2} \leq 2\delta + |\gamma|$  for positive  $\delta$ , the convergence rate for a symmetric perturbation is less or equal to that for an asymmetric perturbation with the same  $|\frac{\delta}{\gamma}|$ . In the two cases corresponding to the one-term models, the convergence rates become independent of whether the perturbation is symmetric or asymmetric,

$$\tilde{r} = \begin{cases} \frac{|\gamma|}{\beta + \gamma - \alpha} & \text{for } |\gamma| \gg \delta, \\ \frac{2\delta}{\beta + \gamma - \alpha} & \text{for } |\gamma| \ll \delta, \end{cases} \quad (48)$$

where the convergence rate for  $|\gamma| \gg \delta$  already has been obtained [Eq. (39)].

Comparing Eq. (47) and the expression for the norms of the critical points given in Eqs. (21) and (26), it is noted that there is a

simple relation between the smallest norm of the critical points and the rates of convergence,

$$\tilde{r} = \frac{1}{\min(|z_+^c|, |z_-^c|)}. \quad (49)$$

To test how accurately  $\tilde{e}^{(n)}(+, |\frac{\delta}{\gamma}|)$  reproduces the large-order behavior of  $|e^{(n)}(+, |\frac{\delta}{\gamma}|)|$ , we have in Fig. 2 included the former function for  $|\frac{\delta}{\gamma}| = 0.25$  and 2. The simple geometric progression of  $\tilde{e}^{(n)}(+)$  does obviously not reproduce the short-range patterns. For the behavior over many orders,  $\tilde{e}^{(n)}(+, 2)$  provides a good match for  $|e^{(n)}(+, 2)|$  but is less accurate for the slower increasing function  $|e^{(n)}(+, 0.25)|$ . However, the deviations between  $\tilde{e}^{(n)}(+, 0.25)$  and the maxima of  $|e^{(n)}(+, 0.25)|$  do not reflect a fundamental flaw of Eq. (47) but rather that the asymptotic region in this case requires higher orders. Similar results are obtained for the expansions for asymmetric perturbations. We will therefore use the identifications in Eq. (47) also for the convergence rate  $r$  of Eq. (41) and use these in Sec. VIII to extract information about  $\gamma$  and  $\delta$  from observed rates of convergence.

## VI. ADDITIONAL ARCHETYPES FOR SYMMETRICAL PERTURBATIONS

### A. The interspersed zigzag archetype: $|\gamma| < |\delta|$

#### 1. The function $e^{(n)}(+, |\frac{\delta}{\gamma}|)$ for $|\frac{\delta}{\gamma}| > 1$

We will first consider the archetype that occurs when the gap-shift is smaller than the coupling term but not so much smaller that the zigzag curve of the one-term model shows up for all considered orders. To examine the behavior of the corrections for this archetype, we consider the plots of  $|e^{(n)}(+, |\frac{\delta}{\gamma}|)|$  in Fig. 2 for the highest plotted values of  $|\frac{\delta}{\gamma}|$ . For  $|\frac{\delta}{\gamma}| = 50$ , each even order gives rise to a larger increase in  $|e^{(n)}(+, |\frac{\delta}{\gamma}|)|$  than its neighbor odd orders so the curve has a zigzag form. The difference between an even order and the surrounding odd orders becomes less pronounced as the order increases and the curve approaches a geometric sequence. For  $|\frac{\delta}{\gamma}| = 10$ , the graphs exhibit the zigzag behavior for the lower orders, a nearly geometric behavior from order 10 to about order 25, and from order 25, the zigzag behavior reoccurs. This archetype is therefore called the interspersed zigzag archetype. All the considered curves have a dominating (2+, 2-) sign-pattern with a few occurrences of three corrections of the same sign in the intervals where the function fluctuates.

To understand the observed features of  $e^{(n)}(+, |\frac{\delta}{\gamma}|)$ , we recall from Sec. IV B that  $e^{(n)}(+, |\frac{\delta}{\gamma}|)$  for  $|\frac{\delta}{\gamma}| > 1$  and lower orders are dominated by the terms  $e_i^{(n)}(+, |\frac{\delta}{\gamma}|)$  with largest  $i$ . We will therefore introduce a model that approximates  $e^{(n)}$  by the sum of the two numerically largest terms in Eq. (12),  $e^{(n)} \approx e_{[\frac{n}{2}]}^{(n)} + e_{[\frac{n}{2}]-1}^{(n)}$ . Considering the even and odd orders separately, one obtains from Eqs. (13) and (14)

$$e^{(n)}\left(\sigma, \left|\frac{\delta}{\gamma}\right|\right) \approx (-\sigma)^{\frac{n}{2}} \frac{(n-2)!\delta^n}{\gamma^n} \times \left( \frac{1}{\left(\frac{n}{2}\right)!\left(\frac{n-1}{2}\right)!} - \frac{\sigma}{2\left(\frac{n-1}{2}\right)!\left(\frac{n-2}{2}\right)!} \left(\frac{\gamma}{\delta}\right)^2 \right) = (-\sigma)^{\frac{n}{2}} \frac{(n-2)!\delta^n}{\left(\frac{n}{2}\right)!\left(\frac{n-1}{2}\right)!\gamma^n} \left( 1 - \frac{\sigma n(n-2)}{8} \left(\frac{\gamma}{\delta}\right)^2 \right), \quad n \text{ even}, \quad (50)$$

$$e^{(n)}\left(\sigma, \left|\frac{\delta}{\gamma}\right|\right) \approx (-\sigma)^{\frac{n-1}{2}} \frac{(n-2)!\delta^{n-1}}{\left(\frac{n-1}{2}\right)!\left(\frac{n-3}{2}\right)!\gamma^{n-1}} \times \left( 1 - \frac{\sigma(n-1)(n-3)}{24} \left(\frac{\gamma}{\delta}\right)^2 \right), \quad n \text{ odd}. \quad (51)$$

By comparing Eqs. (50) and (51), it is noticed that the relative contributions from the second term is about a factor three times larger for a given even order than for the neighboring odd orders. Deviations from the one-term model will therefore first show up for even orders.

An expression for the largest order,  $n_1$ , for which the one-term expression holds may be obtained from Eqs. (50) and (51). We define that the one-term expression holds until the contributions of the second term changes the total term by 50%. As it is the even corrections that have the largest relative contributions from the second term, we use Eq. (50) to identify  $n_1$  for symmetric and asymmetric perturbations as

$$\frac{1}{2} = \frac{n_1(n_1-2)}{8} \frac{\gamma^2}{\delta^2}. \quad (52)$$

Using the approximation  $n_1(n_1-2) \approx (n_1-1)^2$  holding for large  $n_1$ , we obtain the identification

$$n_1 = 1 + 2 \left| \frac{\delta}{\gamma} \right| \approx 2 \left| \frac{\delta}{\gamma} \right|. \quad (53)$$

We next consider the relative changes of  $|e^{(n)}|$  when going between even and odd orders. For  $n$  even, one obtains from Eqs. (50) and (51)

$$\left| \frac{e^{(n+1)}}{e^{(n)}} \right| = (n-1) \left| \frac{1 - \frac{\sigma(n-1)^2}{24} \left(\frac{\gamma}{\delta}\right)^2}{1 - \frac{\sigma(n-1)^2}{8} \left(\frac{\gamma}{\delta}\right)^2} \right| \approx n, \quad (54)$$

$$\left| \frac{e^{(n+2)}}{e^{(n+1)}} \right| = \frac{4\left(\frac{\delta}{\gamma}\right)^2}{n+2} \left| \frac{1 - \frac{\sigma(n+1)^2}{8} \left(\frac{\gamma}{\delta}\right)^2}{1 - \frac{\sigma(n-1)^2}{24} \left(\frac{\gamma}{\delta}\right)^2} \right| \approx \frac{4}{n} \left(\frac{\delta}{\gamma}\right)^2, \quad (55)$$

where the approximate forms are obtained by only retaining the terms that are dominating for lower orders, thereby recovering the zigzag archetype of Sec. IV B.

It is seen from Eqs. (54) and (55) that  $\left| \frac{e^{(n+1)}}{e^{(n)}} \right|$  is the smallest of the two ratios for low orders but increases for increasing orders. In contrast,  $\left| \frac{e^{(n+2)}}{e^{(n+1)}} \right|$  is largest at low orders but decreases for an increasing order. These trends have already been noticed at the one-term level but are enhanced by the inclusion of the second term. These developments of the relative sizes of even and odd

corrections explain the observed changes from pronounced zigzag to geometric or nearly geometric progression in the plots in Fig. (2) for  $\left| \frac{\delta}{\gamma} \right| > 1$ . The observed dominating  $e(2+, 2-)$  sign-patterns for the lowest orders follow directly from the form of  $e_i^{(n)}$  in these intervals; see Eq. (34).

An important feature of the plots of  $e^{(n)}$  in Fig. (2) for  $\left| \frac{\delta}{\gamma} \right| = 2, 4$  and 10 is the recurrence of the zigzag patterns. In the first recurrence of the zigzag pattern, the even-ordered terms become much smaller than the surrounding odd-order terms. This occurs when the order is so large that the two terms in Eq. (50) cancel each other. A similar cancellation for the odd order terms is observed at higher orders for  $\left| \frac{\delta}{\gamma} \right| = 2$  and 4. The orders  $n_e^*, n_o^*$  where the two terms cancel for even and odd orders, respectively, are obtained using the approximations  $n(n-2) \approx (n-1)^2$  in Eq. (50) and  $(n-1)(n-3) \approx (n-2)^2$  in Eq. (51)

$$n_e^* = 1 + \sqrt{8} \left| \frac{\delta}{\gamma} \right| \quad (n^* \text{ even}), \quad (56)$$

$$n_o^* = 2 + 2\sqrt{6} \left| \frac{\delta}{\gamma} \right| \quad (n^* \text{ odd}). \quad (57)$$

It is noted that the order at which the sum of the two odd terms vanishes is roughly twice the order at which the sum of the two even orders vanishes.

Consider  $\left| \frac{\delta}{\gamma} \right| = 2$  as an example of this behavior. In Fig. 4, we plot  $e^{(n)}(+, 2)$  on a logarithmic scale. The upper panel contains the standard curve where consecutive orders are connected, whereas the lower panel contains separate curves for even and odd orders. The cancellations of the two dominating terms for even and odd terms are predicted from Eqs. (56) and (57) to be at orders 6 and 11, respectively. This is in good agreement with the plot, where the first zigzag pattern of even corrections occurs at the order 6 and 8, whereas the first zigzag pattern of the odd corrections occurs at orders 13 and 15. Between the regions with the zigzag pattern, the functions change in a nearly geometric fashion. This pattern of geometric behavior interchanging with regions with zigzag behavior recurs for the higher orders. It is seen from the lower panel that the curves of the even and odd corrections are much smoother than the curve connecting even and odd corrections. As the  $e$ -function, in general, is a fast rising function, the curves on the lower panel do not exhibit minima but rather regions, where the increase is significantly lower than the overall geometric increase.

Concerning the signs, the geometric parts of the curves will have the  $(2+, 2-)$  sign pattern of  $e_i^{(n)}$  for fixed  $i$ . Around the occurrence of the first zigzag pattern, the factor  $1 - \frac{n(n-2)}{8} \left(\frac{\gamma}{\delta}\right)^2$  in Eq. (50) changes sign from positive to negative, and this leads to an additional sign change and thereby to three consecutive orders with the same sign. As the order increases further, the  $(2+, 2-)$  pattern recurs until the next zigzag region, where an additional sign changes arising from a new term in  $e^{(n)}(+, \left| \frac{\delta}{\gamma} \right|)$  becoming dominating. In the example in Fig. 4, we thus observe that  $e^{(n)}(+, 2)$  have constant signs in at the three orders 6, 7, and 8 and again at orders 13, 14, and 15.

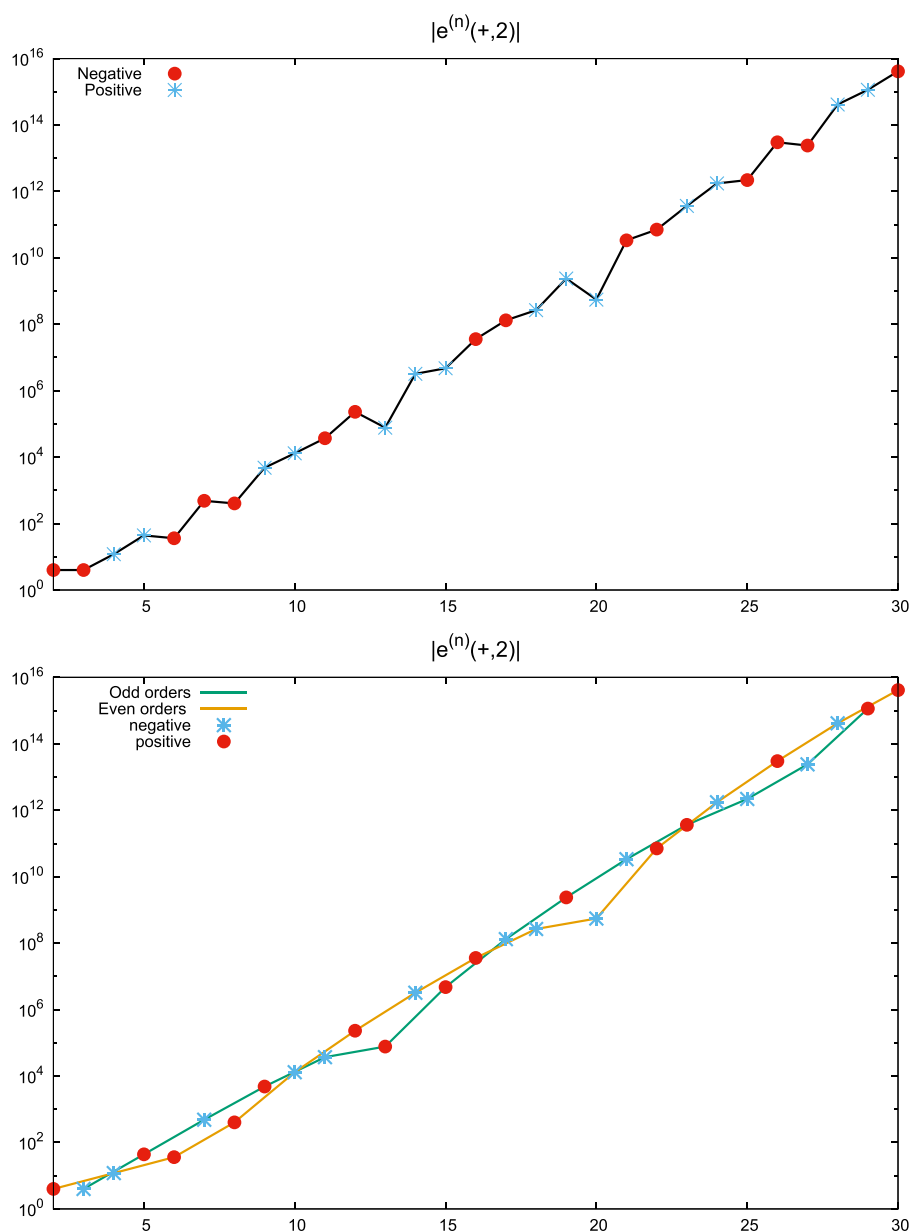


FIG. 4. The function  $e^{(n)}(+, 2)$ . The lower panel gives separate curves for even and odd values of  $n$ .

## 2. Energy corrections

We next consider the full energy corrections of Eq. (11). The ratio between two consecutive energy-corrections equals the ratio between two consecutive  $e$ -term times a constant

$$\frac{E^{(n+1)}}{E^{(n)}} = \frac{\gamma}{\beta + \gamma - \alpha} \frac{e^{(n+1)}}{e^{(n)}}. \quad (58)$$

For orders, where  $e^{(n)}$  is a geometric progression,  $|E^{(n)}|$  is therefore also a geometric progression, and for orders, where  $|e^{(n)}|$  has the zigzag form,  $|E^{(n)}|$  will also have the zigzag form. However, the

prefactor may change the appearance of the zigzag part of the pattern. With respect to the sign-patterns, a positive gap-shift will lead to the same pattern as  $e^{(n)}(+)$ —a dominating  $(2+, 2-)$  pattern alternating with three corrections of the same sign in the zigzag regions. For a negative phase-shift, the pattern of the corrections is obtained by multiplying the pattern of  $e^{(n)}(+)$  and the  $(1+, 1-)$  pattern of the prefactor, leading to the  $(2+, 2-)$  pattern in the geometric and parts of the zigzag regions plus a single occurrence of a sign in the zigzag regions.

As an example of the behavior of the full energy-corrections for  $|\frac{\delta}{\gamma}| > 1$ , we consider in Fig. 5 the corrections up to order 50

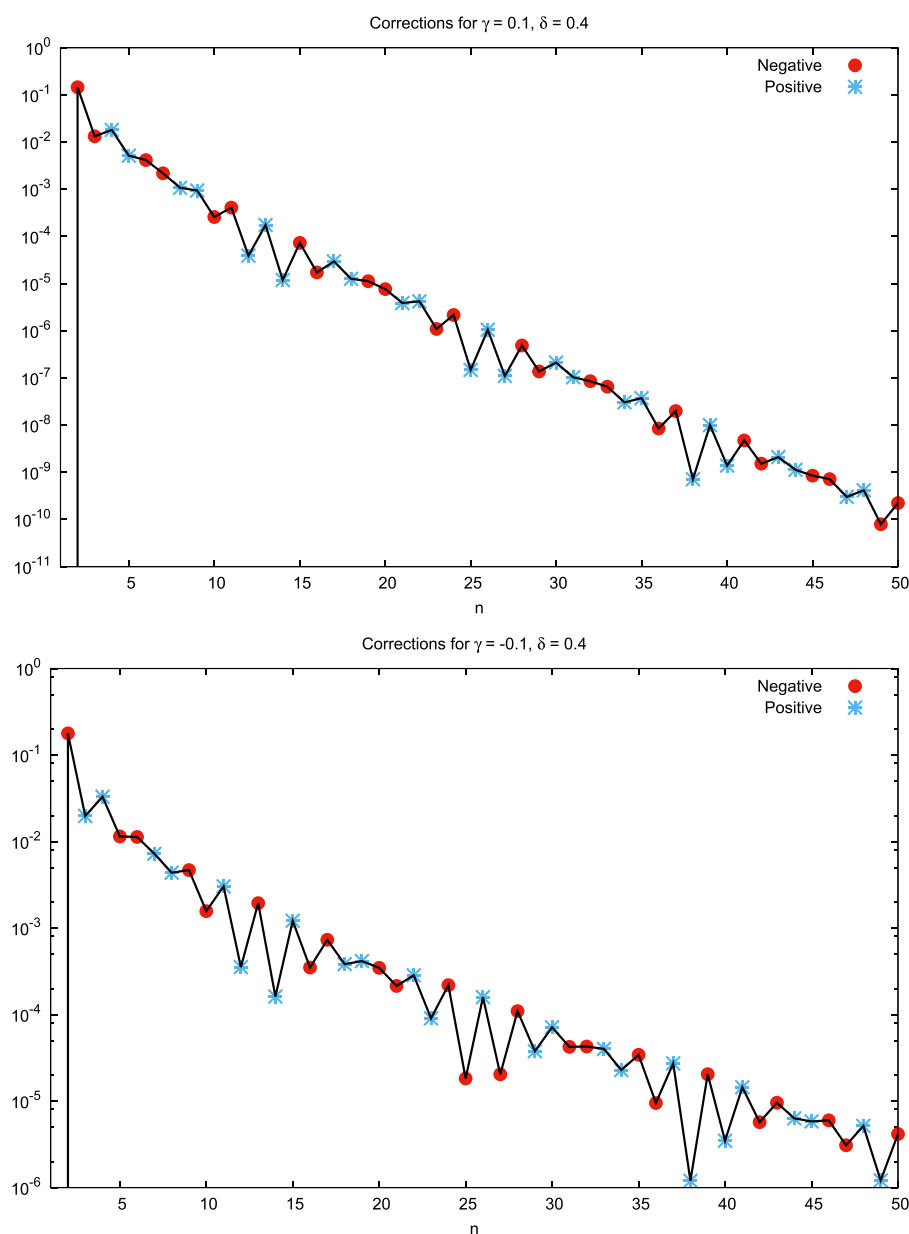


**FIG. 5.** Corrections for a symmetric perturbation with  $\delta = 0.4$ ,  $\gamma = 0.1$  in the upper panel and  $\gamma = -0.1$  in the lower panel.

for the coupling constant 0.4 and two choices of gap-shifts, 0.1 and  $-0.1$ . The rate of convergence is obtained from Eq. (47) as 0.73 and 0.90 for the gap-shifts 0.1 and  $-0.1$ , respectively. Thus, although the corresponding function  $e^{(n)}(+, 4)$  in Fig. 2 is rapidly increasing for increasing  $n$ , the prefactors approach zero so fast that the energy corrections will converge toward zero. The forms of  $E^{(n)}$  for  $\gamma = 0.1$  in the upper panel of 4 and  $E^{(n)}$  for  $\gamma = -0.1$  in the lower panel match as expected that of  $e^{(n)}(+, 4)$  seen in Fig. 2. It is also noted that the rapid reduction in the prefactor leads to zigzag patterns of the energy corrections with much larger fluctuations than  $e^{(n)}(+, 4)$ . This archetype where intervals with dominating even or

odd corrections are interspersed with intervals with nearly geometric convergence is denoted as the interspersed zigzag archetype.

The signs of the corrections in the figure also follow our analysis. In the geometric and parts of the zigzag regions, one observes the  $(2+, 2-)$  pattern, which is intercepted in the zigzag region by three corrections of the same sign for positive gap-shifts and the single occurrence of a sign for negative gap-shifts.

To further illustrate the convergence behavior for zigzag and interspersed zigzag archetypes and the transition between these archetypes, Fig. 6 gives the corrections up to order 50 for the coupling constant of 0.4 and the gap-shifts 0.001, 0.005, 0.02, 0.05,



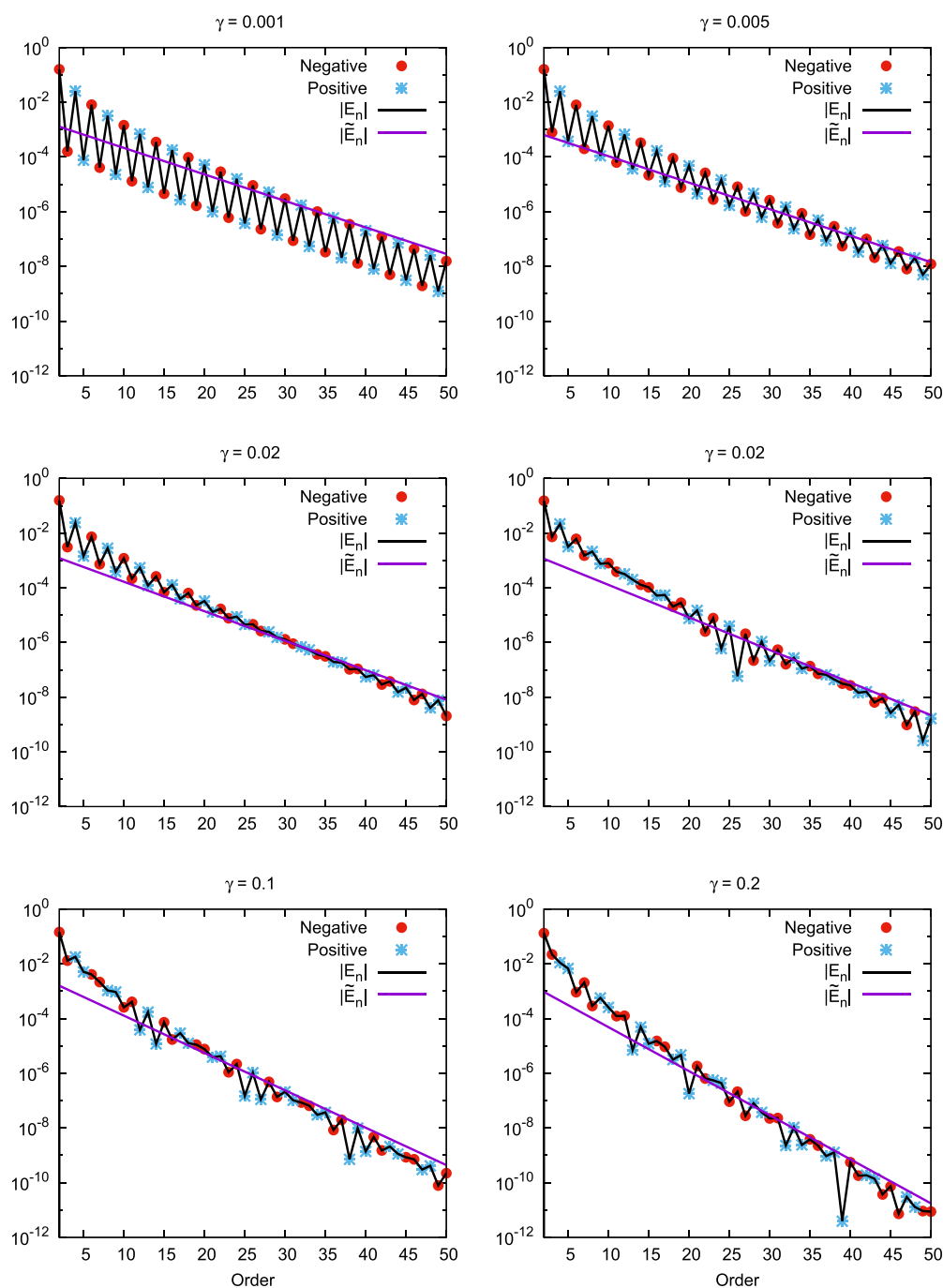


FIG. 6. Absolute corrections for a symmetric perturbation and  $\delta = 0.4$  and  $\gamma < \delta$ .

0.1, and 0.2. The corresponding geometric series of Eq. (43) are also included. For the smallest choices of the gap-shift, 0.001 and 0.005, Eq. (53) shows that the energy corrections to the considered 50 orders behaves as the zigzag archetype and this is apparent in the figure. For the gap-shift 0.02, the zigzag behavior of the

corrections is followed around order 25 by a part where the even and odd terms nearly follow a single geometric progression until the even order terms after order 35 becomes smaller than the neighboring odd orders. For the larger gap-shifts, 0.05, 0.1, and 0.2, we observe the complete interspersed zigzag pattern.

A summary of the interspersed zigzag archetype is given in the first column of Table II. This archetype is observed for  $|\delta| > |\gamma|$  when the considered orders are significantly larger than  $n_1$  of Eq. (53). Intervals of orders where corrections and deviations have a zigzag form interchange with intervals where the corrections follow a nearly geometric sequence. The (2+, 2-) sign pattern is dominating for the corrections and deviations, but in the interval around the local minima, both corrections and deviations show a single occurrence of one or three orders with the same sign for negative or positive values of the gap-shifts, respectively. Furthermore, by comparing the curves for the corrections and the deviations, it is seen that the minima of the absolute deviations typically occur in regions where the absolute corrections show a simple monotonic convergence.

## B. The triadic archetype: $|\gamma| \approx |\delta|$

We next consider the case where the gap-shift and coupling constant have identical or nearly identical size. For such choices of  $\gamma$  and  $\delta$ , the expansion of  $e^{(n)}$  in Eq. (12) must include all terms.

### 1. The function $e^{(n)}(+, 1)$

For  $|\gamma| = |\delta|$ , the expression for the energy corrections in Eq. (11) becomes

$$E^{(n)} = \frac{\gamma^n}{(\beta + \gamma - \alpha)^{n-1}} e^{(n)}(+, 1), \quad |\gamma| = |\delta|. \quad (59)$$

To understand the convergence pattern for this type, we consider the function  $e^{(n)}(+, 1)$  as plotted in Fig. 2. Although the function  $e^{(n)}(+, 1)$  has an irregular behavior, it shows a pattern with a period of three. The terms in each period have a given sign, so the curve is dominated by the sign pattern (3+, 3-). Another reoccurring feature of a single period is that  $e^{(n)}(+, 1)$  typically increases significantly in the first two orders of the period, whereas the third order exhibits either a limited increase or a decrease. In addition to the pattern with a period of three, the curve also has a secondary pattern spanning 17 orders. Thus, the pattern between order 10 and 26 is repeated between order 27 and 44.

### 2. Energy corrections

To examine how the structure of  $e^{(n)}(+, 1)$  in Fig. 2 is folded with the prefactor to give the overall convergence patterns, we give in Fig. 7 the absolute corrections for several positive values of  $\gamma = \delta$ . The vertical line-segments from third to fifth order are caused by the vanishing fourth order corrections. It is seen that the minima that, in general, occur at every third order of  $e^{(n)}(+, 1)$  leads to similar minima of  $E^{(n)}$ . As the absolute corrections exhibit a typical period of three, we will denote this pattern as the triadic archetype. For prefactors that decrease fast for increasing orders, this fast convergence may mask the minima of the triadic behavior as seen in Fig. 7 for several of the periods for  $\gamma = \delta = 0.2$ .

We next consider the signs of the corrections. For positive values of the gap-shift, it is seen from Eq. (59) that the sign of the corrections equals that of  $e^{(n)}(+, 1)$ , so the corrections also have the

(3+, 3-) pattern. For negative values of the gap-shift, the same equations show that the signs of the corrections are obtained by multiplying the (1+, 1-) pattern of the prefactor with the (3+, 3-) pattern of  $e^{(n)}(+, 1)$ , which is readily seen to give a (2+, 1-) or a (1+, 2-) pattern. These sign-patterns are easily recognized in the plots of Fig. 7.

The asymptotic rates of convergence for the three cases considered in Fig. 7 are from Eq. (47) obtained as  $r = 0.37, 0.74$ , and  $1.18$  for  $\gamma = \delta = 0.2, \gamma = \delta = 0.5$ , and  $\gamma = \delta = 1.0$ , respectively. Lines with the stated slopes can be aligned with the maxima of the corrections of Fig. 7. This is illustrated in Fig. 7 where the function  $\tilde{E}^{(n)}$  for  $\delta = \gamma = 0.5$  is plotted with the multiplicative constant chosen, so  $\tilde{E}^{(n)}$  matches the maxima at the highest orders. The lower orders exhibit again a convergence that is faster than predicted by the asymptotic convergence rate.

A summary of the convergence patterns for the triadic archetype is given in the middle column of Table II. If the expansions are slowly convergent or divergent, each instance of the pattern contains two corrections of similar size and a third correction that is much smaller. For a positive gap-shift, the signs of the corrections are constant in a period and changes from one period to the next, leading to a dominating (3+, 3-) sign pattern. If the gap-shift is negative, a (2+, 1-) or a (1-, 2+) sign pattern is observed for most periods.

## C. The ripple archetype: $|\gamma| > |\delta|$

### 1. The function $e^{(n)}(+, \frac{\delta}{\gamma})$ for $|\frac{\delta}{\gamma}| < 1$

In our discussion of Fig. 2, it was noticed that plots of  $e^{(n)}(+, \frac{\delta}{\gamma})$  with  $|\frac{\delta}{\gamma}| < 1$  for sufficient large orders exhibit ripples, rather than the straight lines predicted by the one-term geometric model of IVC. We therefore denote this archetype as the ripple archetype.

In order to understand the occurrence of the ripples, we extend the one-term analysis of Sec. IV C to include the two terms that for lower orders dominates  $e^{(n)}(+, \frac{\delta}{\gamma})$  for  $|\frac{\delta}{\gamma}| < 1$ ,

$$e^{(n)} \approx e_1^{(n)} + e_2^{(n)} = \left( -\sigma + \frac{(n-2)(n-3)}{2} \frac{\delta^2}{\gamma^2} \right) \frac{\delta^2}{\gamma^2}. \quad (60)$$

The relative contribution from the second term increases quadratically when the order is increased.

We first determine for which orders the geometric one-term model is accurate. We define that the one-term model is accurate up to an order  $n_1$ , where the two-term expansion of Eq. (60) deviates at most 50% from the one-term model and obtain the identification

$$\frac{1}{2} = \frac{(n_1-2)(n_1-3)}{2} \frac{\delta^2}{\gamma^2}, \quad (61)$$

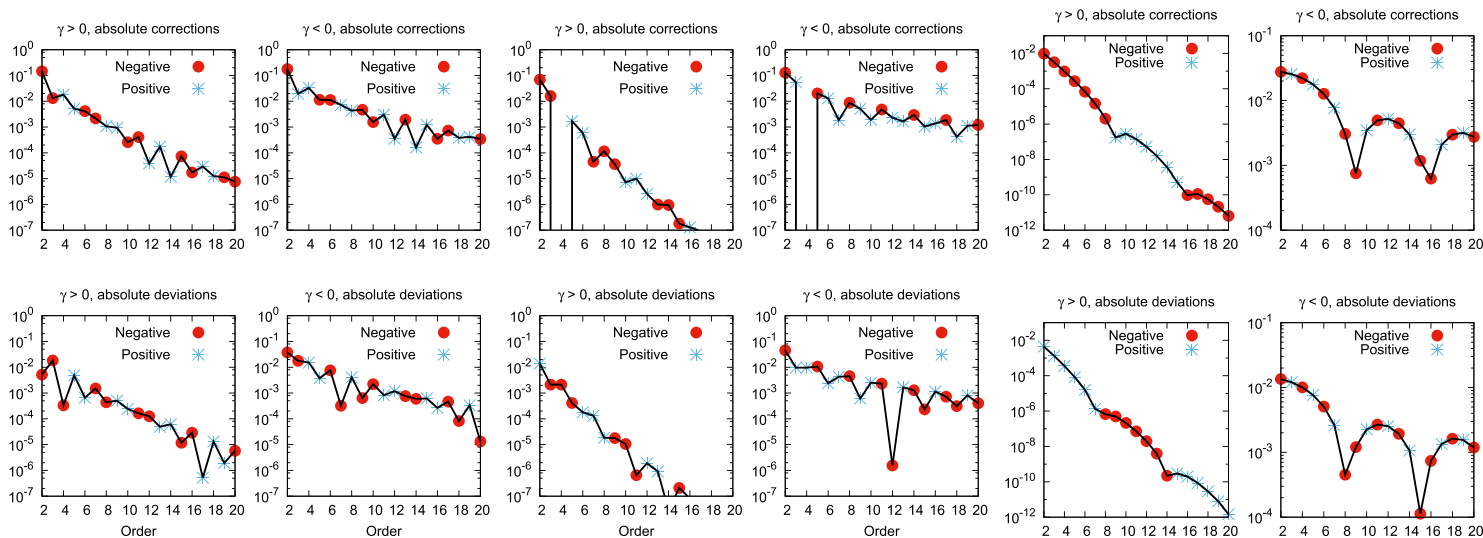
which holds both for symmetric and asymmetric perturbations. Using the approximation  $(n_1-2)(n_1-3) \approx (n_1 - \frac{5}{2})^2$  which holds for  $n_1 \gg 1$ , we obtain the identification

$$n_1 = 2.5 + \left| \frac{\gamma}{\delta} \right| \approx \left| \frac{\gamma}{\delta} \right|. \quad (62)$$

TABLE II. The interspersed zigzag, triadic and ripple archetypes for symmetric perturbations.

Type	Interspersed zigzag	Triadic	Ripple
Identification	$ \gamma  <  \delta $	$ \gamma  \approx  \delta $	$ \gamma  >  \delta $
Period	$n^* = 1 + \sqrt{8} \left  \frac{\delta}{\gamma} \right $	3	$n^* = 2.5 + \sqrt{2} \left  \frac{\gamma}{\delta} \right $
Rate of convergence		$\frac{\sqrt{4\delta^2 + \gamma^2}}{\beta + \gamma - \alpha}$	

Typical form of corrections and deviations



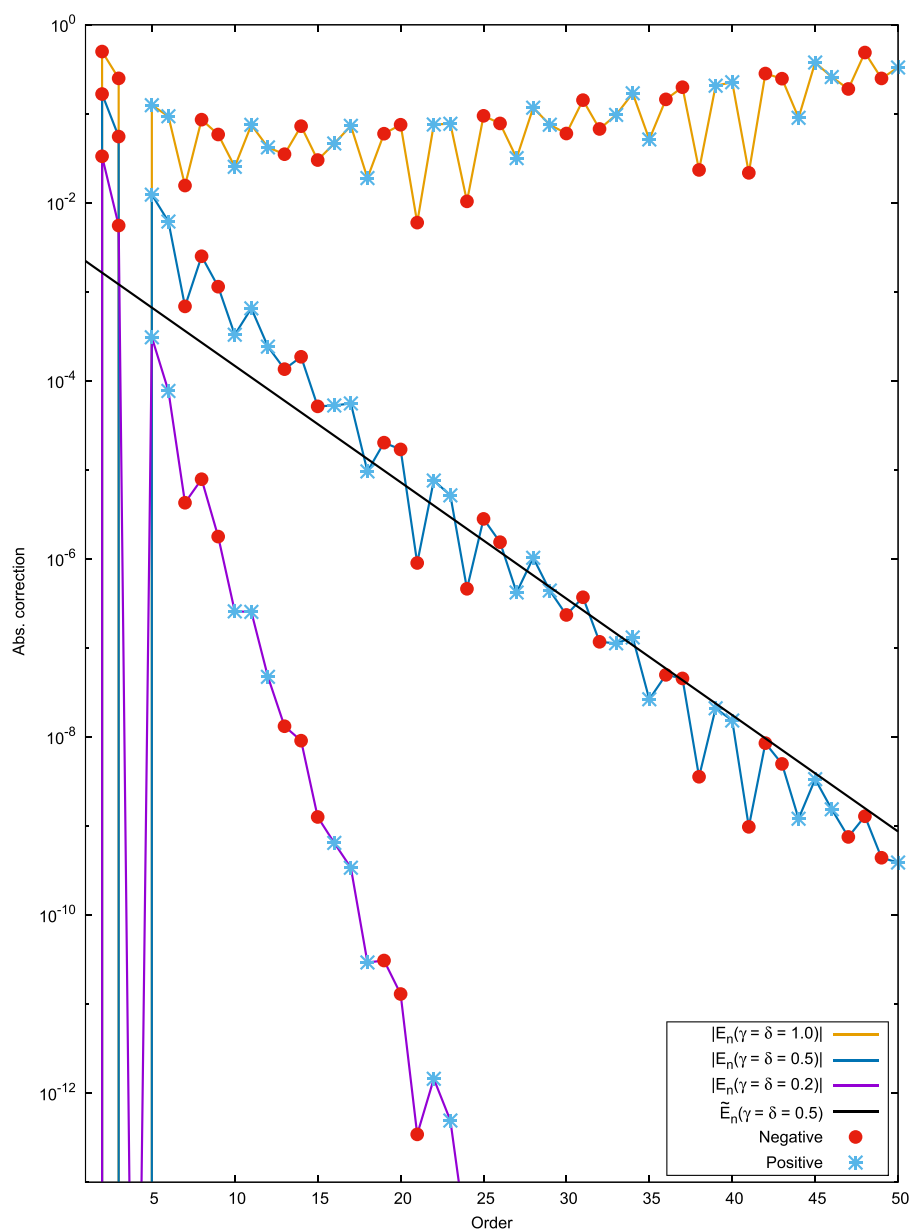


FIG. 7. Absolute corrections for a symmetric perturbation for various choices of  $|\gamma| = |\delta|$ .

As the transition from the geometric to the ripple archetypes is not very precisely defined, we will use the last expression of Eq. (62) for  $n_1$  in the following.

For symmetric perturbations, the second term in Eq. (60) increases in importance when the order increases beyond  $n_1$ . For an order  $n^*$ , the sum of the two terms vanishes and a local minimum of  $|e^{(n)}(+, |\frac{\delta}{\gamma}|)|$  occurs, and this marks the end of the first ripple. From Eq. (60), the value of  $n^*$  may be obtained using  $(n-2)(n-3) \approx (n-\frac{5}{2})^2$  as

$$n^* = 2.5 + \sqrt{2} \left| \frac{\gamma}{\delta} \right|. \quad (63)$$

When  $n$  increases beyond  $n^*$ , the positive  $e_2^{(n)}$  term dominates and the absolute value of  $e^{(n)}$  starts to increase. When the order is further increased, the negative third term,  $e_3^{(n)}$ , becomes significant and reduces  $|e^{(n)}|$  leading to a second minimum, and this pattern continues. A formula for this second minimum may be obtained, but we will only consider the more qualitative aspects for which Eq. (63) gives a good estimate of the periodicity of all the ripples.

The accuracy of using Eq. (63) to determine the period of the ripples may be examined using the plots of Fig. 2 for the relevant values of  $|\frac{\delta}{\gamma}|$ . The periods of the ripples are from Eq. (63) predicted  $|\frac{\delta}{\gamma}| = 0.02, 0.25, 0.4$ , and  $0.5$  to be 73, 8, 6, and 5, whereas Fig. 2

shows that the actual periods are 95, 7, 5, and 4. The predicted and observed periods are thus in fair agreement.

With respect to the signs of  $e^{(n)}$ , it is seen from the above discussion that the signs are constant within a ripple and changes when going from one ripple to the next. The sign pattern of  $e^{(n)}$  is thus  $(n^+ +, n^* -)$  with  $e^{(n)}$  being negative in the first ripple.

## 2. Energy corrections

The full corrections are obtained from  $e^{(n)}(+, \left|\frac{\delta}{\gamma}\right|)$  by multiplying with the geometric prefactor  $\frac{\gamma^n}{(\beta+\gamma-\alpha)^{n-1}}$ , so the ripple structure of

$e^{(n)}(+, \left|\frac{\delta}{\gamma}\right|)$  will also show up for the full energy corrections. With respect to the sign patterns, the prefactor is positive for a positive gap-shift and the energy corrections will have the same  $(n^+ +, n^* -)$  pattern as  $e^{(n)}(+, \left|\frac{\delta}{\gamma}\right|)$ . For a negative gap-shift, the geometric prefactor is an alternating function of  $n$ , so the sign pattern will be  $(1+, 1-)$  within a given period and there will be two consecutive energy corrections with the same sign when going from one ripple to the next.

To illustrate the corrections for the ripple archetype, we consider in Fig. 8 expansions with  $(\gamma, \delta) = (-0.48, 0.12)$  and  $(\gamma, \delta) = (4, 1)$ , corresponding to the fixed ratio  $\left|\frac{\delta}{\gamma}\right| = 0.25$ . From Fig. 2,

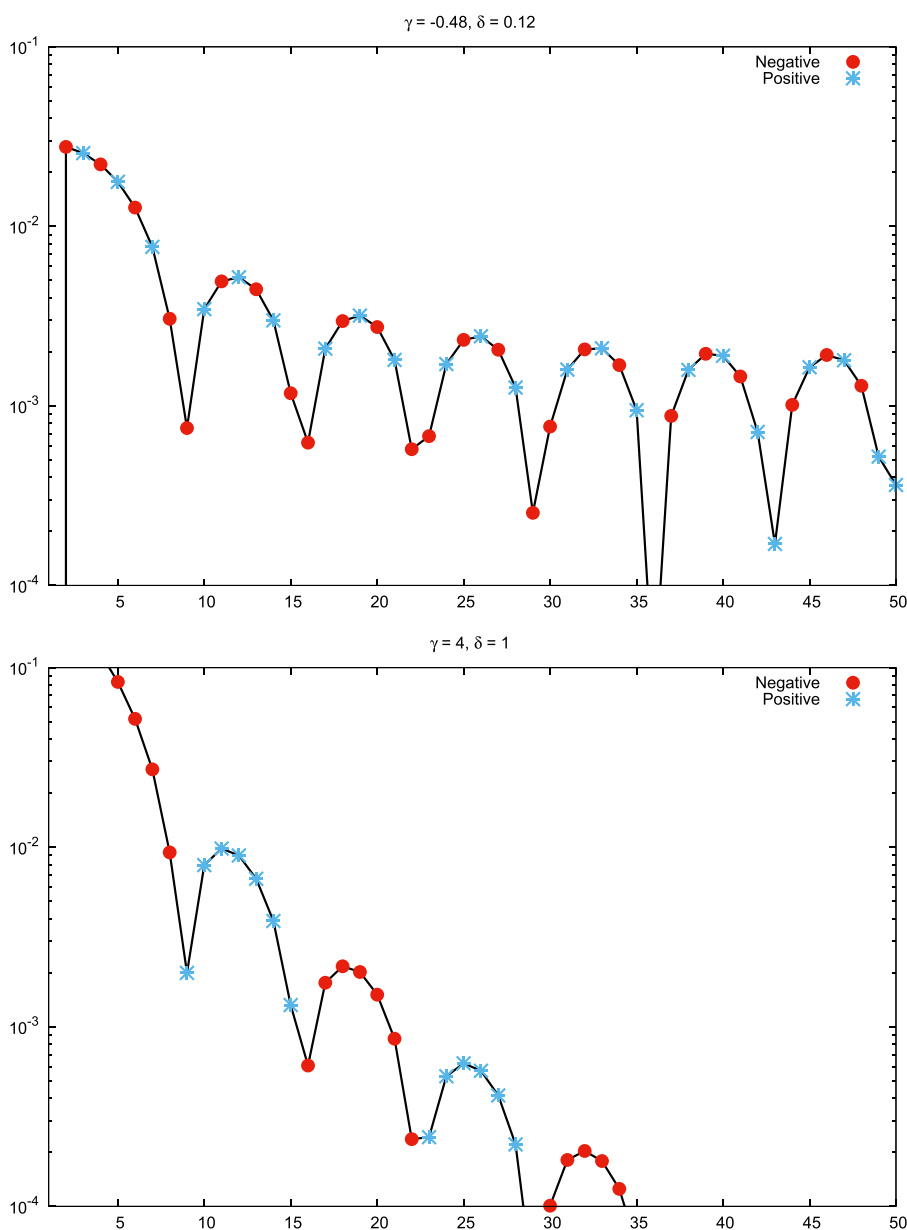


FIG. 8. Corrections for a symmetric perturbation and  $\gamma = -0.48, \delta = 0.12$  (top) and  $\gamma = 4, \delta = 1$  (bottom).

it is seen that  $e^{(n)}(+, 0.25)$  has a dominating period of 7. The curves for the absolute corrections in Fig. 8 show for both parameter sets the expected ripples with the period of 7 and the above developed sign patterns.

A summary of the convergence patterns for the ripple archetype is given in the right column of Table II. The ripples occur with a period that is inverse proportional to  $|\frac{\delta}{\gamma}|$ , and a good estimate of the period is given by Eq. (63). For a positive gap-shift, the sign patterns for both the corrections and deviations are  $(n^*+, n^*-)$  starting with negative corrections and positive deviations. For a negative gap-shift, the corrections and deviations are negative at the second order and have a  $(1+, 1-)$  sign pattern within a ripple. When going from one ripple to the next, there are usually two corrections and deviations of the same sign.

### VII. ADDITIONAL ARCHETYPES FOR THE ASYMMETRIC PERTURBATIONS

We will now consider the archetypes that may arise for an asymmetric perturbation beyond the zigzag and geometric archetypes discussed in Sec. IV. We start by a discussion of the

function  $e^{(n)}(-, |\frac{\delta}{\gamma}|)$  and then introduce two additional archetypes, the convex-geometric and zigzag-geometric archetypes.

#### A. The function $e^{(n)}(-, |\frac{\delta}{\gamma}|)$

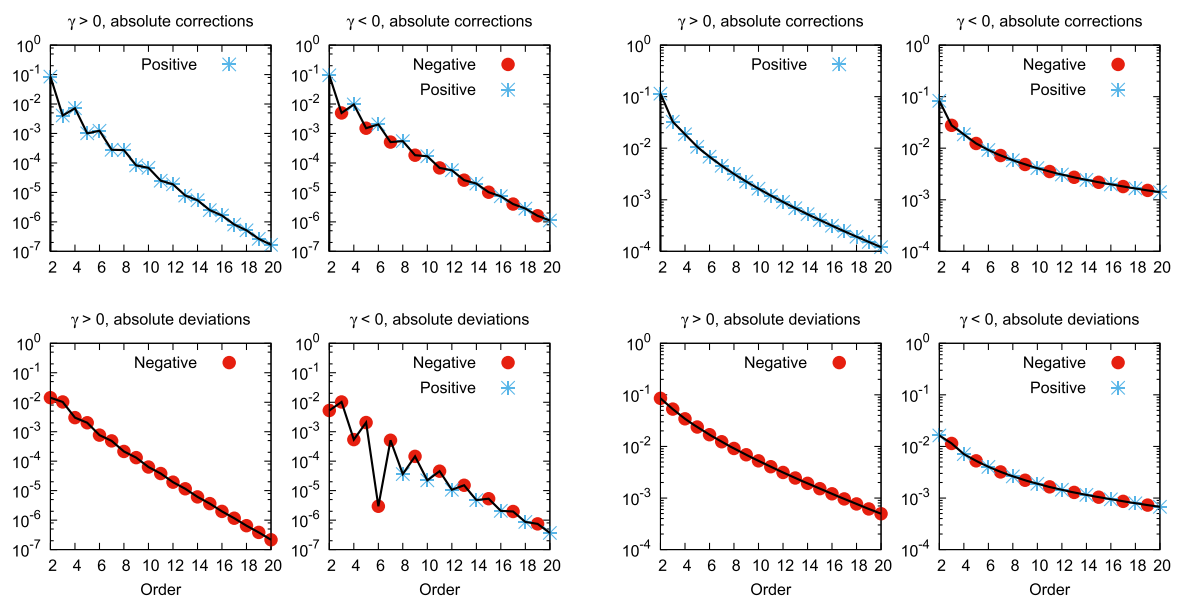
The functions  $e^{(n)}(-, |\frac{\delta}{\gamma}|)$  in Fig. 3 do not show any recurring ripples or zigzag patterns. This is easily understood from Eqs. (12) and (13) which shows that  $e^{(n)}(-, |\frac{\delta}{\gamma}|)$  is a sum of positive numbers. The recurring cancellations of positive and negative terms that give the zigzag and ripple structures for  $e^{(n)}(+, |\frac{\delta}{\gamma}|)$  therefore do not occur for  $e^{(n)}(-, |\frac{\delta}{\gamma}|)$  and  $e^{(n)}(-, |\frac{\delta}{\gamma}|)$  become instead a geometric expansion for sufficient large order.

At lower orders, the form of  $e^{(n)}(-, |\frac{\delta}{\gamma}|)$  depends on the value of  $|\frac{\delta}{\gamma}|$ . Three forms of  $e^{(n)}(-, |\frac{\delta}{\gamma}|)$  are observed: a form for very small values of  $|\frac{\delta}{\gamma}|$ , where the function is a geometric progression from the start; a form for values of  $|\frac{\delta}{\gamma}|$  around one, where the function is convex for lower orders and geometric for higher orders; and

TABLE III. The zigzag-geometric and convex-geometric archetypes for asymmetric perturbations.

Type	Zigzag-geometric	Convex-geometric
Identification	$ \gamma  <  \delta $	$ \gamma  \geq  \delta $
Rate of convergence	$r = \frac{2\delta +  \gamma }{\beta + \gamma - \alpha}$	

#### Typical form of corrections and deviations



finally a form with larger values of  $\left|\frac{\delta}{\gamma}\right|$ , where the functions have a zigzag form for lower orders and a geometric form for higher orders.

## B. The convex-geometric and the zigzag-geometric archetypes

The two additional forms of  $e^{(n)}(-, \left|\frac{\delta}{\gamma}\right|)$  give rise to two new archetypes for the energy-corrections: the zigzag-geometric and the convex-geometric archetypes. The structure and sign-patterns for these archetypes are summarized in Table III.

The zigzag-geometric archetype is observed when  $\left|\frac{\delta}{\gamma}\right|$  is larger than one and when orders larger than or comparable to  $n_1$  of Eq. (53) are considered. For orders smaller than  $n_1$ , the corrections exhibit zigzag forms, and when the order approaches  $n_1$ , the corrections approach a geometric series.

The convex-geometric archetype is observed when  $\left|\frac{\delta}{\gamma}\right|$  is equal or not much smaller than 1 and shows a convex curve of corrections for lower orders and a geometric curve for larger orders.

For both of the new archetypes, the sign patterns of the corrections are identical and equal to the sign patterns of the prefactor since  $e^{(n)}(-, \left|\frac{\delta}{\gamma}\right|)$  is positive. The corrections have therefore the (1+, 1-) sign pattern for negative gap-shifts and the (1+) pattern for positive gap-shifts.

Table III also contains plots of the deviations for the two additional archetypes. For the zigzag-geometric archetype, the deviations in the zigzag part of the curve exhibit the sign patterns of the zigzag archetype, whereas the geometric part has the sign pattern of the geometric archetype. For a negative shift, there is thus a noticeable difference in the sign patterns of the corrections and deviations. The corrections have the (1+, 1-) sign pattern for all orders with the even-ordered corrections being positive, whereas the signs of the deviations shift from a (1-) to a (1+, 1-) pattern when the convergence changes from the zigzag to the geometric form for increasing orders. Positive gap-shifts lead to deviations that are negative in both parts of the curves. The deviations for the convex-geometric archetype have the same sign patterns as the standard geometric archetype: the deviations have the same sign as the corrections for a negative gap-shift, and the deviations are negative for a positive gap-shift.

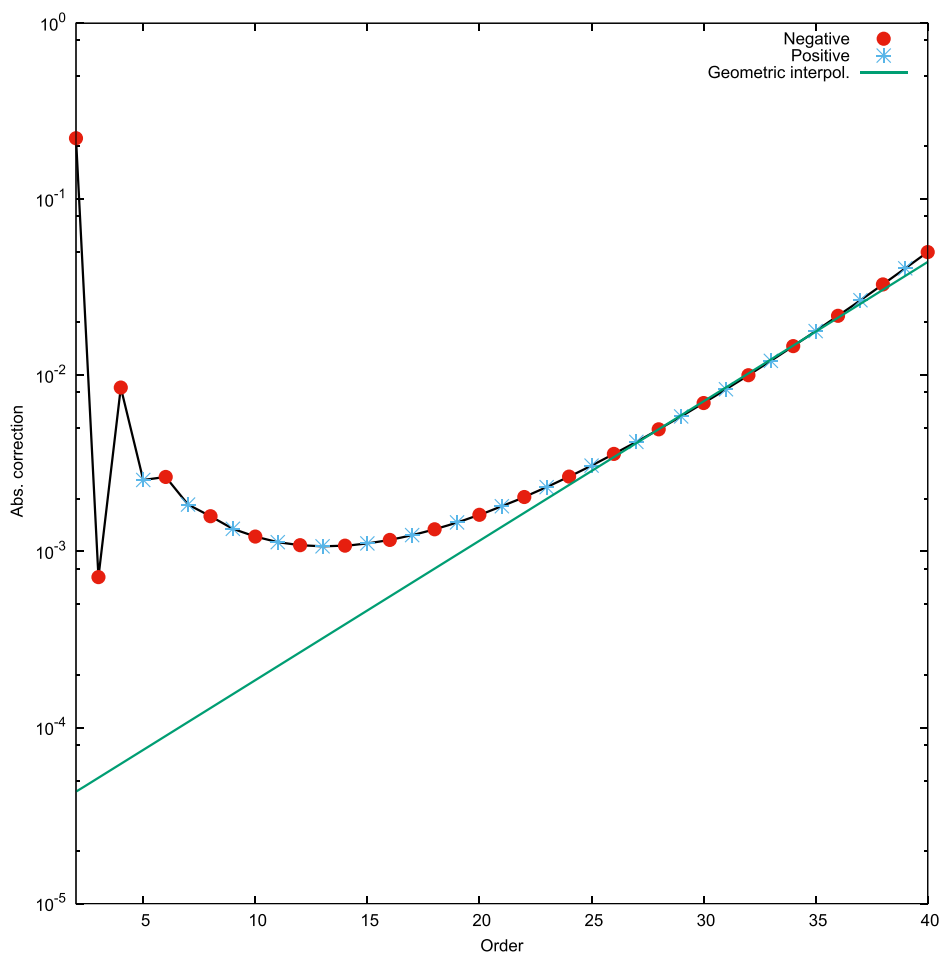


FIG. 9. The MPPT series (in a.u.) for HF using the aug-cc-pVDZ basis set. An example of the geometric archetype with a negative gap-shift.

## VIII. EXAMPLES OF ARCHETYPICAL FORMS OF CONVERGENCE IN MPPT AND COUPLED CLUSTER PERTURBATION THEORY

We will now consider examples of perturbation expansions of ground state and excitation energies and show how the archetypes developed for the two-state problem show up in the higher orders of these expansions. In addition to standard MPPT calculations, we consider CCPT<sup>14</sup> and CP expansions.<sup>16,18</sup> We have not encountered expansions, where the size of the coupling is so much larger than the gap shift that the zigzag archetype is encountered. For the remaining archetypes for symmetric perturbations and for the zigzag-geometric archetype for asymmetric perturbations, we have encountered several examples and discuss in the following representative cases.

### A. A perturbation calculation of the geometric archetype

Both MPPT and CPPT expansions use the Fock-operator as the zeroth-order Hamiltonian and have therefore large differences between the full and the zeroth-order energies, which imply that the gap-shifts are large. We therefore expect that MPPT and CPPT

expansions typically have either the geometric or ripple archetypes. In many of these expansions, the coupling is rather small, so the periods of the ripples will be larger than the calculated orders and the archetypes will then appear as geometric progressions.

Consider as an example the MPPT series for the HF molecule at using the aug-cc-pVDZ basis and the bond distance 0.916 Å. The corrections for this expansion are plotted in Fig. 9. It is seen that the corrections reduce in size until order 13 from where the expansion diverges. From order 25, the corrections exhibit the geometric progression and the archetype of the expansion is therefore geometric. Since the corrections have alternating signs, the gap-shift is negative and the intruder state is a back door intruder. From the geometric interpolation given in the figure, a rate of convergence of about 1.2 is estimated. Inserting this rate of convergence into the second equation of Eq. (39), one obtains  $\gamma_s = 0.55$ . In Ref. 21, the explicit form of the two-state Hamiltonian was determined and the obtained parameters are  $\beta - \alpha = 12.32$ ,  $\gamma = -7.07$ , and  $\delta = -0.00034$ . The scaled gap shift is thus  $\gamma_s = -7.07/12.32 = 0.57$ , which is in good agreement with the value obtained from the plot. Inserting the above values into Eq. (63), the period of the ripples is obtained as about 22,000, which is beyond the largest order carried out in MPPT benchmark calculations.

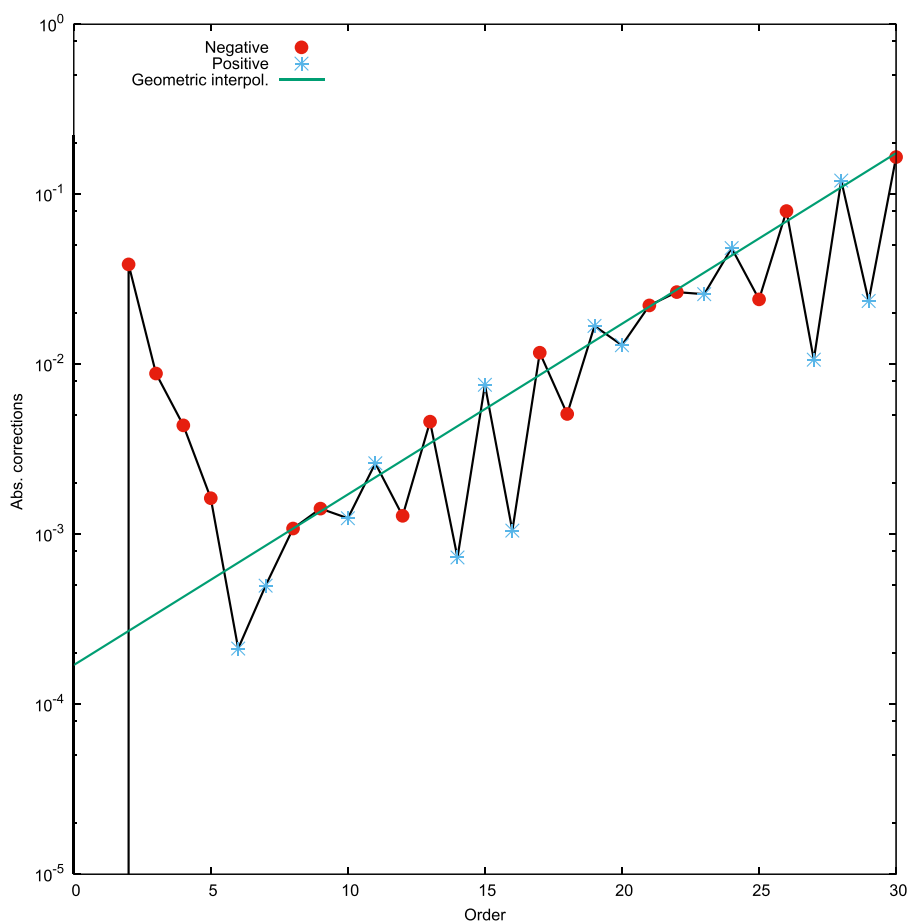


**FIG. 10.** The CPST(T) series (in a.u.) for the excitation energy to the first excited  $^1A_1$  state for  $\text{CH}_2$ . An example of the interspersed zigzag archetype with a positive gap-shift.



## B. A perturbation calculation of the interspersed zigzag archetype

We next consider in Fig. 10 the CP calculation for the excitation energy to the lowest excited singlet state of symmetry  $A_1$  of  $\text{CH}_2$  in the cc-pVDZ basis with the coupled-cluster single double (CCSD) state as the parent state and the coupled-cluster single double triple (CCSDT) state as the target state.<sup>17</sup> The overall structure of the curve is similar to the curve in the upper panel of Fig. 5: intervals with nearly geometric progression alternate with intervals where there are marked differences between the magnitude of the even and odd corrections, so the convergence archetype is the interspersed zigzag archetype. The signed corrections have three consecutive corrections with the same sign in the regions with local minima of the absolute corrections, so the gap-shift is positive according to Table II.

The minima of the absolute corrections occur at orders 14 and 27, corresponding to a period of about 13 orders. Using this value for the period, we estimate from Eq. (56) that  $\frac{\delta_s}{\gamma_s} \approx 4$ . A convergence rate of 1.23 is obtained from the line in Fig. 10 connecting two points in the regions of geometric progression. Combining this value of the convergence rate with the estimate of  $\frac{\delta_s}{\gamma_s}$ , we obtain from Eq. (C6) that  $\gamma_s$  is about 0.17 and thereby  $\delta_s \approx 0.7$ .

In this case, the divergence is caused by the large coupling. A closer examination of the various corrections to the excitation operator shows that the dominating part of these are in the CCSD space, so the divergence is caused by the interactions between two states in the parent space. The gap-shift is rather small as the energies of both states are described accurately in the parent space.

## C. A perturbation calculation of the triadic archetype

As an example of a perturbation expansion of the triadic archetype, we give in Fig. 11 the corrections for the CPSD(T-n) calculation on the excitation energy to the second excited  ${}^3B_2$  state of  $\text{CH}_2$  using the cc-pVDZ basis.<sup>17</sup> From the sixth order, the signs are dominated by the (3+, 3-) pattern, with a few period of length 2 and 4. According to the examples given in Table II, the sign of  $\gamma$  is therefore positive. The curve has another telltale of the triadic archetype: the minimum or small increase in the size of the corrections that shows at every third order starting at order 15. Obviously, it is not likely that the underlying perturbation has exact identical values of  $\gamma_s$  and  $\delta_s$ , but the similarity to the behavior for the triadic archetype indicates that the two parameters are nearly

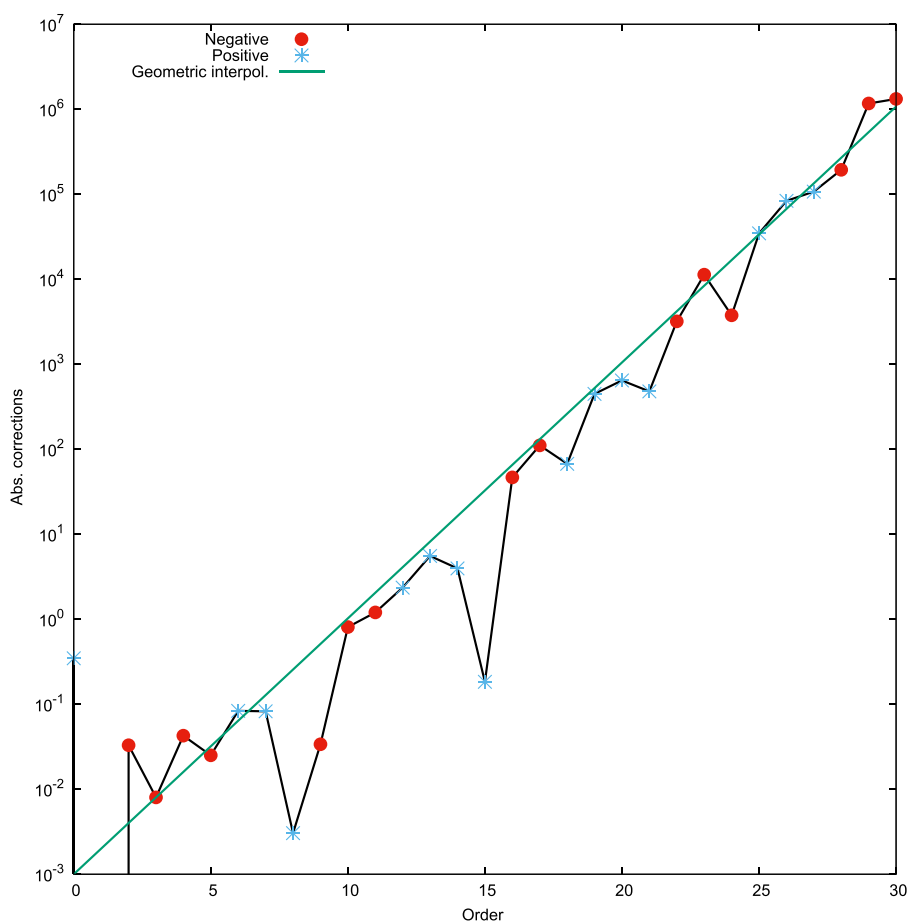


FIG. 11. The CPSD(T) series (in a.u.) for the second excited  ${}^3B_2$  state. An example of the triadic archetype with a positive gap-shift.

identical. The figure contains also a geometric approximation to the corrections and shows that the large scale behavior of the corrections are well approximated with a simple geometric expansion. The rate of convergence is obtained as about two. Taking this value of the rate constant and assuming that  $\gamma = \delta$ , one obtains from Eq. (47) that  $\gamma_s = \delta_s \approx 8$ , so the values of the parameters are much larger than the value of about 0.8 that according to Eq. (47) gives the convergence rate of 1 and thereby the largest value for which the triadic expansion converges.

#### D. A perturbation calculation of the ripples archetype

The  $C_2$  molecule has a low-lying excited state arising from the double excitation  $2\sigma_u^2 \rightarrow 3\sigma_g^2$ , and the presence of this excited state gives a large coupling in the asymptotic two-state problem and thereby to an MPPT series that deviates from geometric convergence at lower orders. Previous MPPT calculations on this molecule showed that the corrections have multiple ripples.<sup>10,12</sup> The MPPT corrections for this molecule at the internuclear distance of 2.348 bohrs using the cc-pVDZ basis are given in Fig. 12.

It is observed from Fig. 12 that the corrections exhibit the ripple archetype for orders larger than 10 and that the curve of corrections from this order is similar to the curve of corrections for the two-state model in Fig. 8 with  $\gamma = -0.48$ ,  $\delta = 0.12$ . Inside the ripples, the corrections have alternating signs, so the gap-shift is negative according to the examples of Table II. From Fig. 12, it is seen that ripples have a period of 9. Using this value for the period, Eq. (63) gives a ratio  $|\frac{\gamma_s}{\delta_s}|$  of 4.6. From a linear fit to the three maxima for the highest orders, one obtains the rate of convergence of 0.93 for the geometric interpolation also given in the figure. Using this value for the rate of convergence, one obtains from Eq. (C6) that  $\gamma_s = -0.46$  and thereby  $\delta_s = 0.1$ . The value of the scaled gap-shift is therefore close to the critical value of  $-0.5$  [see Eq. (23)]. The determined rate of convergence of 0.93 is so low that even if the asymptotic convergence rate is approached from below, we predict that the expansion is convergent. This is in agreement with the calculations in Ref. 12, where the corrections were calculated to order 150 and showed a convergent trend. From the identifications of  $\gamma_s$  and  $\delta_s$ , it is concluded that it is the underestimate of the energy difference in zeroth order between the ground and the doubly excited state that leads to the slow convergence rather than the large coupling between the states.

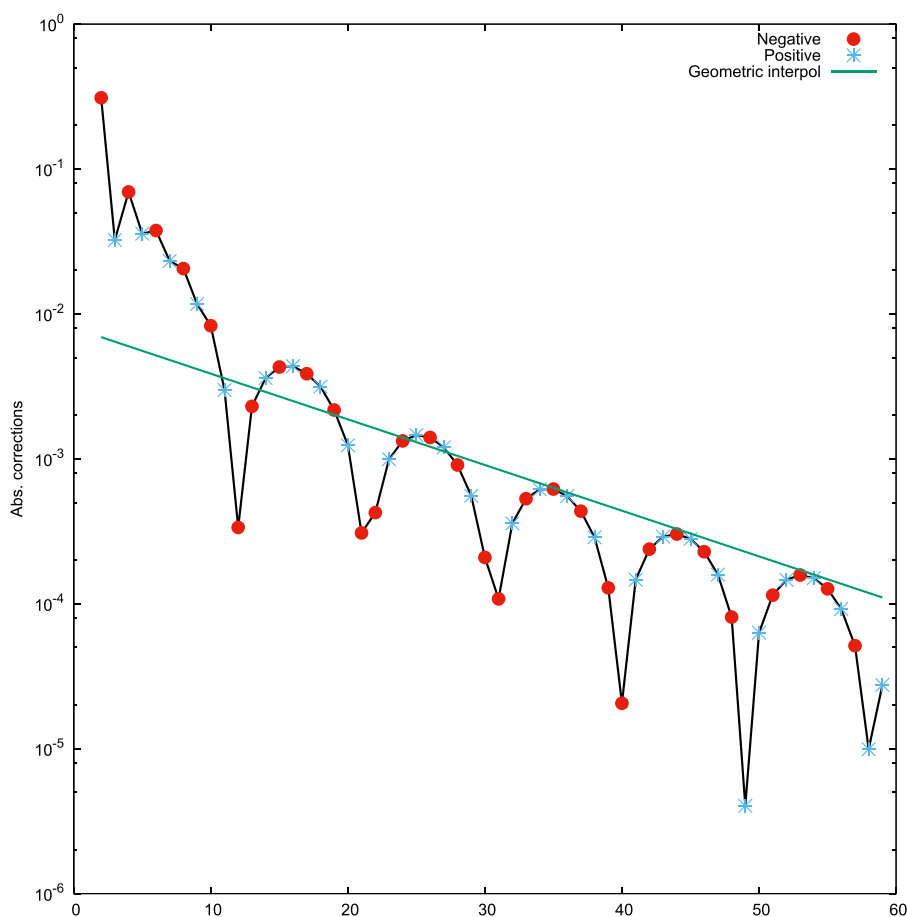
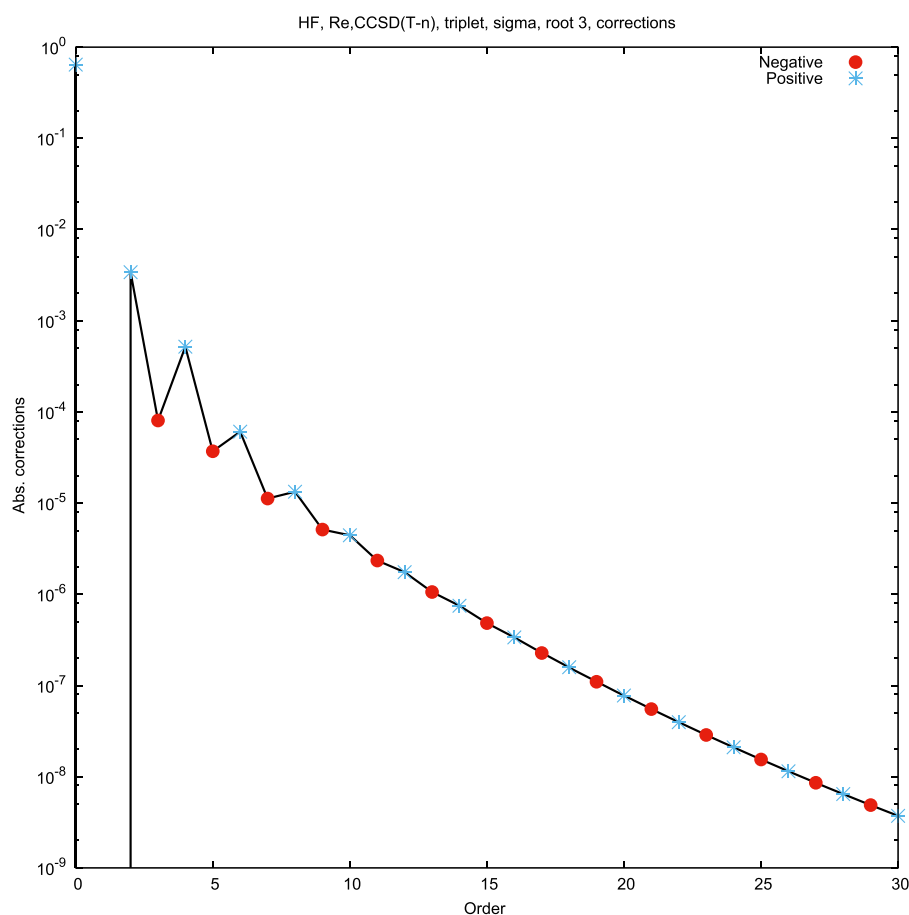


FIG. 12. The MPPT series (in a.u.) for  $C_2$ . An example of the ripples archetype with a negative gap-shift.



**FIG. 13.** The CPSD(T) series (in a.u.) for the third  $^3\Sigma$  state of HF at  $R_e$ . An example of the zigzag geometric archetype with a negative gap-shift.

### E. A perturbation calculation of the zigzag-geometric archetype

As an example of the convergence behavior corresponding to an asymmetric perturbation, we consider the CPSD(T-n) hierarchy for the third  $^3\Sigma$  state for HF at the equilibrium geometry using the aug-cc-pVDZ basis set.<sup>17</sup> The corrections for this calculation are given in Fig. 13. Comparing with the archetypes of Table III, it is seen that this calculation corresponds to a two-state problem of the zigzag-geometric archetype with a negative gap-shift. The first 10 corrections exhibit the zigzag form, which then progress to a nearly geometric convergence from around order 15. If the division between the zigzag and the geometric form is set to order 15, we have from Eq. (53) that  $\left|\frac{\delta}{\gamma}\right|$  is of about 15. The geometric interpolation curve based on the higher order corrections is also given in the figure and gives an asymptotic rate of convergence of 0.74. Using this convergence rate together with the obtained value of 15 for  $\left|\frac{\delta}{\gamma}\right|$ , Eq. (47) gives  $\gamma_s \approx -0.02$  and  $\delta_s \approx 0.3$ . As expected for a zigzag-geometric archetype, the convergence of the expansion is defined by a large coupling constant.

### IX. DISCUSSION AND CONCLUSION

We have extended our previous analysis of perturbation expansions of the two-state problem and its use to rationalize and describe nondegenerate perturbation expansions for electron correlation. To allow for an analysis of coupled cluster perturbation expansions and other perturbation methods with a non-Hermitian perturbation, the analysis has been extended to a general, not necessarily Hermitian, real two-dimensional model perturbation matrix. It is shown that a two-dimensional perturbation matrix where the two off-diagonal elements have the same sign may be re-expressed as a standard symmetric perturbation expansion containing the geometrically averaged off-diagonal element. Similarly a perturbation matrix containing two off-diagonal elements with opposite signs leads to the same corrections as obtained for a symmetric perturbation expansion containing off-diagonal elements of the same size, but opposite signs. It is therefore only when the two off-diagonal elements have opposite signs that the deviations from a Hermitian perturbation leads to new forms of perturbation expansions.

A general two-dimensional general perturbation may therefore be defined in terms of three parameters: the coupling term, which is the size of the off-diagonal element; the symmetry factor,

which describes whether the two off-diagonal elements have identical or opposite signs; and the gap-shift, which describes the perturbation correction to the difference between the two zeroth-order energies.

For a symmetric perturbation, we find that the convergence patterns may be grouped in five archetypes: zigzag, interspersed zigzag, triadic, ripples, and geometric. These five archetypes are traversed when the coupling changes from a size that is much larger than the gap-shift to a size that is much smaller than the gap-shift. For each of the five archetypes, the interplay between the various terms in the perturbation leads to a characteristic pattern. A previous analysis<sup>21</sup> for the special case of the geometric convergence has thereby been extended to all possible archetypes that may be encountered for the symmetric two-state perturbation expansion. For an asymmetric perturbation, there are two additional archetypes: the zigzag-geometric and the convex-geometric. The properties and typical convergence patterns of the seven archetypes are summarized in Tables I–III.

A number of studies have examined MPPT expansions through high order for different molecules and basis sets; see Refs. 8, 10, 12, and 21. The most typical archetype for MPPT expansions is the geometric type, but the ripples archetype occurs for a few cases. We have here shown that the MPPT expansion for  $C_2$  that in Ref. 12 was referred to as “a fascinating pattern of protracted decayed ringing” is an example of the ripple archetype. The remaining three archetypes for symmetric perturbations, zigzag, interspersed zigzag, and triadic have not been observed in MPPT calculations. The absence of these patterns from MPPT expansions may be traced to use of the Fock-operator as the zeroth-order Hamiltonian. Thus, the large differences between diagonal matrix elements of the Fock-operator and of the full Hamiltonian imply that gap-shifts for MPPT are large and much larger than the coupling, which leads to the typically observed geometric archetype.

In recent years, perturbation methods that use coupled cluster states rather than HF reference states as the parent state and where the target state is an coupled cluster state with a larger excitation level have been developed. The recently introduced CP group of perturbation methods<sup>16</sup> is an example of such expansions and is distinct from other methods by the use of a zeroth-order Jacobian that contains the full Jacobian in the parent subspace. In the CP method, relative energies are therefore accurately described already at zero order for states belonging to the parent space. For expansions, where the high-order convergence is dominated by corrections in the parent space, the coupling is therefore often larger than the gap-shift, and the archetype becomes the interspersed zigzag type. Furthermore, as the CP perturbation matrix is not symmetric, the generalization of the two-state model to contain asymmetric off-diagonal elements is needed to describe these perturbation methods. For the CP expansions for excitation energies, we have thus encountered examples of the interspersed zigzag, triadic, ripple, geometric, and zigzag-geometric archetypes.

We find thus that the total of seven archetypes of convergence behavior do not only define the possible forms of convergence for the two-state problem, but they also contain the possible high-order convergence patterns for actual perturbation calculations, even when these contain expansions over millions of states. This implies that the primary critical point of the perturbation expansion defines the high-order convergence, irrespectively

of whether this point is inside or outside the complex unit-circle. This is in line with the previous observations<sup>3,21</sup> that the high-order corrections to the wave function approaches a one-dimensional space. Under the assumption that the various contributions to the corrections may be considered as independent, this finding is explained by Eq. (49) as these then shows that it is the state corresponding to the primary critical point that has the slowest convergence.

It is natural to question which archetypes will be observed for the convergence of multireference perturbation methods. Since the most commonly used zeroth-order Hamiltonians for these expansions<sup>24,25</sup> includes the Fock-operator, we expect that these expansions will belong to the geometric or ripple archetypes. This is in line with the results of previous high-order multireference perturbation expansions.<sup>5,26</sup>

Although the developed formulas and concepts have been able to describe all the perturbation expansions that we hitherto have encountered, there are some limitations in our treatment that should be mentioned. The first of these is that we have focused on the convergence of the root that has the lowest zero-order state as the reference state. However, the second order and higher order corrections for the higher root are easily obtained by changing the sign of the corrections for the investigated lower root.<sup>19</sup> This simple sign-change is most easily shown by observing that the sum of the two eigenvalues in Eq. (6) contains terms in  $z$  that are at most linear. We did also assume that the diagonal of the full two-dimensional Hamiltonian had the same numerical order as the zeroth-order Hamiltonian. This retainment of order holds for typical perturbation expansions but is obviously not universal. The number of archetypes and their overall appearance do not depend on this assumption, but the detailed form of the convergence rates and radii of convergence do depend on this assumption. The form of these for situations where the numerical ordering of the diagonals changes when going from the zero-order to the full Hamiltonian is currently being studied. Another possible extension is to consider a two-dimensional perturbation problem where both the matrix elements are allowed to be general complex numbers. This adds, however, significant complexity to the problem. A somewhat more fundamental line of investigation would be a more detailed mathematical analysis of the recurrence of the various patterns of the archetypes. Although our treatment does explain the recurrences, we strongly suspect that a more detailed mathematical analysis will be able to explain the nearly constant length of the periods over many recurrences.

In addition to improved understanding of the two-state model *per se*, it is also important to obtain an improved understanding of why the high-orders of perturbation expansions in a finite dimensional space seems to be well described by a two-dimensional space. For many iterative methods, such as the power method for determining extreme eigenvalues, it is simple to show that the asymptotic behavior is determined by two eigenvectors. However, perturbation expansions are not simple repetitions of the same procedure, and a mathematical sound proof for the conditions under which the asymptotic convergence is described by a space containing two vectors is absent. Along the same line, exactly what are the characteristics of the two vectors? In many calculations on excitation energies using the cluster perturbation methods, the two-dimensional space is spanned by two states that each are solutions

to the full problem,<sup>19</sup> but it is far from certain that this holds, in general.

Finally, it is interesting to use the identification of the parts of the perturbation that lead to the slow convergence to modify the splitting of the Hamiltonian into a zeroth-order and perturbation part during the iterative procedure to obtain faster convergence. For example, the geometric and the ripples archetypes indicate that the diagonal gap-shift is much larger than the coupling, so convergence can probably be improved by moving a part of the gap-shift from the perturbation to the zeroth-order Hamiltonian. For the zigzag and the interspersed zigzag archetypes, the course of the slow convergence is the coupling between the two zero-order states, so in this case, a modified perturbation expansion should be obtained by rotating the two zero-order states to obtain a perturbation with a smaller coupling. Research along these directions is currently being pursued, but the practical use is expected to be limited as one, in general, only calculates the lowest orders.

Even with the above limitations, we expect that the present analysis of the various convergence types of perturbation expansions and of their relation to the dominating parts of the perturbation will improve our understanding of existing perturbation methods and provide useful insights that can contribute to future developments.

## ACKNOWLEDGMENTS

The research was supported by Grant No. DFF - 4181-00537 from the Danish Research Council (FNU) to J.O.

## APPENDIX A: DEFECTIVE MATRICES OF DIMENSION TWO

In this appendix, we consider a general two-dimensional matrix,

$$A = \begin{pmatrix} A_{11} & A_{12} \\ A_{21} & A_{22} \end{pmatrix}, \quad (\text{A1})$$

and show that it is defective, i.e., the space of eigenvectors is one-dimensional, only if it has a single eigenvalue and at most one of the off-diagonal elements are nonvanishing. The eigenvalues of  $A$  are readily obtained as

$$E_{\pm} = \frac{A_{11} + A_{22}}{2} \pm \frac{\sqrt{(A_{11} - A_{22})^2 - 4A_{12}A_{21}}}{2}. \quad (\text{A2})$$

Consider first the case where the discriminant  $(A_{11} - A_{22})^2 - 4A_{12}A_{21}$  is nonvanishing, so  $A$  has two different eigenvalues. As there always is at least one eigenvector for each eigenvalue, the matrix has two eigenvectors and is not defective. Consider next the case where  $(A_{11} - A_{22})^2 - 4A_{12}A_{21} = 0$  is corresponding to a single eigenvalue,  $\frac{A_{11} + A_{22}}{2}$ . The discriminant may be vanishing if  $4A_{12}A_{21} \neq 0$  and  $A_{21} = \frac{-(A_{11} - A_{22})^2}{4A_{12}}$  or if  $4A_{12}A_{21} = 0$  and  $A_{11} = A_{22}$ . Using an unnormalized form of the eigenvector,  $\begin{pmatrix} 1 \\ x \end{pmatrix}$ , the eigenvector equation for the first case reads

$$\begin{pmatrix} A_{11} & A_{12} \\ \frac{-(A_{11} - A_{22})^2}{4A_{12}} & A_{22} \end{pmatrix} \begin{pmatrix} 1 \\ x \end{pmatrix} = \frac{A_{11} + A_{22}}{2} \begin{pmatrix} 1 \\ x \end{pmatrix}, \quad (\text{A3})$$

which identifies

$$x = \frac{A_{22} - A_{11}}{2A_{12}}, \quad (\text{A4})$$

so there is only a one-dimensional eigenvector space, and the matrix is defective. In case  $A_{11} = A_{22}$  and only one of the off-diagonal elements, for example,  $A_{21}$  is vanishing, the eigenvector equation reads

$$\begin{pmatrix} A_{11} & A_{12} \\ 0 & A_{11} \end{pmatrix} \begin{pmatrix} 1 \\ x \end{pmatrix} = A_{11} \begin{pmatrix} 1 \\ x \end{pmatrix}, \quad (\text{A5})$$

which identifies

$$x = 0. \quad (\text{A6})$$

It is readily shown that there are no eigenvectors of the form  $\begin{pmatrix} x \\ 1 \end{pmatrix}$ , and the space of eigenvectors for this case is again one-dimensional. The only remaining case is the trivial degenerate and diagonal case, where  $A_{11} = A_{22}$  and  $A_{12} = A_{21} = 0$ . In this case, both  $\begin{pmatrix} 1 \\ 0 \end{pmatrix}$  and  $\begin{pmatrix} 0 \\ 1 \end{pmatrix}$  are eigenvectors, so the eigenvector-space is two-dimensional.

## APPENDIX B: DEVIATION FOR $\gamma = 0$

To determine the deviation as defined in Eq. (32), we use the Lagrange form of the remainder,<sup>23</sup> which states that the remainder of a Taylor-expansion,  $f^n(x)$ , obtained by expanding a function  $f(x)$  through order  $n$  around  $x_0$  may be written as

$$f(x) - f^n(x) = \frac{|x - x_0|}{(n+1)!} f^{(n+1)}(\xi), \quad (\text{B1})$$

where  $\xi$  is in the interval between  $x$  and  $x_0$ . In the current context, it is noted from Eq. (6) that  $E_-(z)$  for  $\gamma = 0$  may be written as a function of  $z^2$ ,

$$E_-(z^2) = \frac{\alpha + \beta}{2} - \frac{\beta - \alpha}{2} \sqrt{1 + \frac{4\sigma\delta^2}{(\beta - \alpha)^2} z^2}. \quad (\text{B2})$$

The sum  $\sum_{i=0}^{2n} E^{(i)}$  for  $\gamma = 0$  is therefore equal to the Taylor expansion of  $E_-(z^2)$  at  $z^2 = 1$  expanded through order  $n$  in  $z^2$  around  $z^2 = 0$ . The  $n$ -th derivative of the function  $f(x) = \sqrt{1+x}$  for  $n \geq 2$  equals  $(-1)^{n-1} \frac{(2n-3)!!}{2^n}$ , so the deviation in Eq. (32) may be obtained as

$$\begin{aligned} D_{2n} &= \frac{-1}{(n+1)!} \left. \frac{\partial^{n+1} E_-(z^2)}{\partial (z^2)^{n+1}} \right|_{z^2=\xi} \\ &= \frac{\sigma(-\sigma)^n (2n-1)!! 2^n}{(n+1)!} \frac{\delta^{2n+2}}{(\beta - \alpha)^{2n+1}} \sqrt{1 + \frac{4\sigma\delta^2}{(\beta - \alpha)^2} \xi}, \quad \xi \in [0, 1]. \end{aligned} \quad (\text{B3})$$

Since the odd corrections are vanishing for  $\gamma = 0$ , we furthermore have

$$D_{2n+1} = D_{2n}. \quad (\text{B4})$$

### APPENDIX C: EXPRESSIONS FOR THE RATE OF CONVERGENCE FOR $\tilde{e}^{(n)}$ AND $\tilde{E}^{(n)}$

To determine  $p(+, |\frac{\delta}{\gamma}|)$  from Eqs. (44) and (45), we introduce the scaled parameters of Eq. (29) and use Eq. (44) to write Eq. (45)

$$\frac{|\gamma_s|}{1 + \gamma_s} p(+, |\frac{\delta_s}{\gamma_s}|) = 1 \text{ for } \frac{1 + \gamma_s}{\sqrt{4\delta_s^2 + \gamma_s^2}} = 1. \quad (\text{C1})$$

For a given ratio

$$x = |\frac{\delta}{\gamma}| = |\frac{\delta_s}{\gamma_s}|, \quad (\text{C2})$$

there are two choices of  $\gamma_s$  that fulfill the condition on the right-hand side of Eq. (C1)

$$\gamma_s = \frac{1}{\sqrt{4x^2 + 1} - 1}, \frac{-1}{\sqrt{4x^2 + 1} + 1}. \quad (\text{C3})$$

Inserting either of these values into Eq. (C1) identifies

$$p(+, x) = \sqrt{4x^2 + 1}, \quad (\text{C4})$$

which inserted into Eqs. (42) and (43) gives the geometric energy-series as

$$\tilde{e}^{(n)}(+, |\frac{\delta}{\gamma}|) = c_0(+, |\frac{\delta}{\gamma}|) \left( \sqrt{4 \left( \frac{\delta}{\gamma} \right)^2 + 1} \right)^n. \quad (\text{C5})$$

Finally, by introducing Eq. (C4) in the expression for the convergence rate in Eq. (44), we obtain

$$\tilde{r} = \frac{|\gamma|}{\beta - \alpha + \gamma} \sqrt{4 \left( \frac{\delta}{\gamma} \right)^2 + 1} = \frac{\sqrt{4\delta^2 + \gamma^2}}{\beta + \gamma - \alpha}. \quad (\text{C6})$$

In the above development, we tacitly assumed that  $\gamma$  is nonvanishing. For  $\gamma = 0$ , the asymptotic convergence rate is given by Eq. (39), which is equal to the convergence rate obtained from Eq. (C6) by setting  $\gamma = 0$ . We can therefore use the convergence rate of Eq. (C6) for all choices of  $\gamma$ .

For an asymmetric perturbation, the two critical points  $z_-^c, z_+^c$  of Eq. (24) are real and  $\min(|z_-^c|, |z_+^c|)$  is given by Eq. (26). For a fixed value of the ratio  $x$ , we first obtain expressions for the values of the scaled gap-shift,  $\gamma_s$ , for which  $\min(|z_-^c|, |z_+^c|) = 1$ . In terms of  $\gamma_s$  and  $x$ , the smallest norm of the critical points in Eq. (26) become

$$\min(|z_-^c|, |z_+^c|) = \frac{1 + \gamma_s}{(1 + 2x)|\gamma_s|}, \quad (\text{C7})$$

so the condition that the lowest norm of the critical points equals 1 is

$$1 + \gamma_s = (1 + 2x)|\gamma_s| \Rightarrow \min(|z_-^c|, |z_+^c|) = 1. \quad (\text{C8})$$

By separately considering negative and positive values of  $\gamma_s$ , one obtains from Eq. (C8) two possible values of  $\gamma_s$ ,

$$\gamma_s = \begin{cases} \frac{-1}{2+2x} & \text{if } \gamma_s < 0, \\ \frac{1}{2x} & \text{if } \gamma_s > 0. \end{cases} \quad (\text{C9})$$

We next require that the convergence rate of the geometric approximation to the energy-corrections, Eq. (43),

$$\tilde{r} = \left| \frac{\tilde{E}^{(n+1)}}{\tilde{E}^{(n)}} \right| = \frac{|\gamma|}{\beta + \gamma - \alpha} p(-, x), \quad (\text{C10})$$

has the value 1 for the values of  $\gamma_s$  of Eq. (C9). For both positive and negative values of  $\gamma_s$ , one obtains

$$p(-, x) = 2x + 1, \quad (\text{C11})$$

so the geometric approximations to  $e^{(n)}$  for asymmetric perturbations become

$$\tilde{e}^{(n)}(-, |\frac{\delta}{\gamma}|) = c^{(0)}(+, |\frac{\delta}{\gamma}|) \left( 2 \left| \frac{\delta}{\gamma} \right| + 1 \right)^n. \quad (\text{C12})$$

The rate of convergence of the energy corrections  $\tilde{E}^{(n)}$  for an asymmetric perturbation may be obtained from Eqs. (C10) and (C11). Remembering that  $\delta$  is positive, one obtains

$$\tilde{r} = \frac{|\gamma|}{\beta + \gamma - \alpha} \left( 2 \left| \frac{\delta}{\gamma} \right| + 1 \right) = \frac{2\delta + |\gamma|}{\beta + \gamma - \alpha}. \quad (\text{C13})$$

In the above equation, it was again tacitly assumed that  $\gamma \neq 0$ . For  $\gamma = 0$ , we have from Eq. (16) that the absolute corrections are the same for a symmetric and an asymmetric perturbation, so the convergence rate is again given by Eq. (39). The convergence rate of Eq. (C13) reduces to this expression for  $\gamma = 0$  and may therefore be used for all values of  $\gamma$ .

### REFERENCES

- E. Schrödinger, *Ann. Phys.* **385**, 437 (1926).
- C. Møller and M. S. Plesset, *Phys. Rev.* **46**, 618 (1934).
- R. J. Bartlett, *Annu. Rev. Phys. Chem.* **32**, 359 (1981).
- D. Cremer, *Wiley Interdiscip. Rev.: Comput. Mol. Sci.* **1**, 509 (2011).
- T. Helgaker, P. Jørgensen, and J. Olsen, *Molecular Electronic-Structure Theory* (Wiley & Sons, Ltd., West Sussex, UK, 2000).
- T. Kato, *Perturbation Theory for Linear Operators* (Springer-Verlag, New York, 1966).
- F. Rellich, *Perturbation Theory of Eigenvalue Problems*, 1953 New York University Lecture Notes (Gordon and Breach, 1968).
- N. C. Handy, P. J. Knowles, and K. Somasundram, *Theor. Chim. Acta* **68**, 87 (1985).
- D. Cremer and Z. He, *J. Phys. Chem.* **100**, 6173 (1996).
- J. Olsen, O. Christiansen, H. Koch, and P. Jørgensen, *J. Chem. Phys.* **105**, 5082 (1996).
- O. Christiansen, J. Olsen, P. Jørgensen, H. Koch, and P.-Å. Malmqvist, *Chem. Phys. Lett.* **261**, 369 (1996).
- M. L. Leininger, W. D. Allen, H. F. Schaefer III, and C. D. Sherrill, *J. Chem. Phys.* **112**, 9213 (2000).
- J. J. Eriksen, K. Kristensen, T. Kjærgaard, P. Jørgensen, and J. Gauss, *J. Chem. Phys.* **140**, 064108 (2014).
- K. Kristensen, J. J. Eriksen, D. A. Matthews, J. Olsen, and P. Jørgensen, *J. Chem. Phys.* **144**, 064103 (2016).
- J. J. Eriksen, K. Kristensen, D. A. Matthews, P. Jørgensen, and J. Olsen, *J. Chem. Phys.* **145**, 224104 (2016).
- F. Pawłowski, J. Olsen, and P. Jørgensen, *J. Chem. Phys.* **150**, 134108 (2019).
- F. Pawłowski, J. Olsen, and P. Jørgensen, *J. Chem. Phys.* **150**, 134109 (2019).
- P. Baudin, F. Pawłowski, D. Bykov, D. Liakh, K. Kristensen, J. Olsen, and P. Jørgensen, *J. Chem. Phys.* **150**, 134110 (2019).

<sup>19</sup>F. Pawłowski, J. Olsen, and P. Jørgensen, *J. Chem. Phys.* **150**, 134111 (2019).

<sup>20</sup>F. Pawłowski, J. Olsen, and P. Jørgensen, *J. Chem. Phys.* **150**, 134112 (2019).

<sup>21</sup>J. Olsen, P. Jørgensen, T. Helgaker, and O. Christiansen, *J. Chem. Phys.* **112**, 9736 (2000).

<sup>22</sup>R. K. Chaudhuri, J. P. Finley, and K. F. Freed, *J. Chem. Phys.* **106**, 4067 (1997).

<sup>23</sup>M. Abramowitz and I. A. Stegun, *Handbook of Mathematical Functions with Formulas, Graphs, and Mathematical Tables*, 9th ed. (Dover, New York, 1972).

<sup>24</sup>K. Anderson, P.-Å. Malmqvist, B. Roos, and K. Wolinski, *J. Phys. Chem.* **94**, 5483 (1990).

<sup>25</sup>C. Angeli, R. Cimraglia, S. Evangelisti, T. Leininger, and J.-P. Malrieu, *J. Chem. Phys.* **114**, 10252 (2001).

<sup>26</sup>J. Olsen and M. P. Fülcher, *Chem. Phys. Lett.* **326**, 225 (2000).